PHYSICAL REVIEW B VOLUME 19, NUMBER 3 1 FEBRUARY 1979

New theoretical model for transition-metal impurities alloyed in copper, local magnetic moments, and the Kondo effect

K. H. Johnson and D. D. Vvedensky
Department of Materials Science and Engineering, Massachusetts Institute of Technology, Cambridge, Massachusetts 02139

R. P. Messmer
General Electric Corporate Research and Development, Schenectady, New York 12301

(Received 20 June 1978)

Self-consistent-field $X\alpha$ scattered-wave (SCF-$X\alpha$-SW) cluster molecular-orbital models have been constructed for transition-metal impurities (Ni, Fe, Mn, and V) alloyed in crystalline copper, in order to gain insight into the occurrence of local magnetic moments and the Kondo effect, traditionally viewed as many-body effects arising from the interaction of the transition-metal impurities with the conduction electrons of the host metal. A 19-atom cluster representing the local molecular environment, up to second-nearest neighbors, of an isolated transition-metal impurity in an otherwise perfect crystalline copper lattice yields manifolds of molecular-orbital energy levels corresponding to the copper "d band," bracketed by impurity dsp hybrid-orbital energy levels that are bonding with respect to the bottom of the copper d band and antibonding with respect to the top of the d band. The latter cluster orbitals, in conjunction with Hund's rules, (i) are discrete analogs of Friedel-Anderson virtual impurity states, (ii) satisfy a "sum rule" analogous to the Friedel sum rule, (iii) have spin occupancies and polarization in accord with measured magnetic moments, (iv) are consistent with measured trends of residual electrical resistivity, and (v) describe the "renormalizing" effects of the crystalline environment on the transition-metal impurity atom. The most striking result of these theoretical studies is the discovery that local coordination chemical bonding dominates the interaction of the transition-metal impurity with its crystalline environment, yielding a large splitting ($\sim$4–4.5 eV) between bonding and antibonding impurity dsp-hybrid molecular-orbital energy levels and a spin splitting ($\sim$0.2–0.6 eV) of the highest occupied antibonding dsp-hybrid orbitals (the Friedel-Anderson-like impurity states) that is an order of magnitude smaller than values assumed in previous theoretical models (e.g., the Anderson model). The near degeneracy of the latter spin orbitals (for Fe and Mn impurities) with cluster molecular-orbital analogs of the conduction-band eigenstates of crystalline copper near the Fermi energy suggests that the "spin-compensation cloud" often associated with the Kondo effect is considerably smaller in magnetization and more spatially localized around the impurity than assumed in previous formal theories and, in conjunction with the SCF-$X\alpha$ transition-state concept, also provides a discrete orbital basis for discussing the onset of "localized spin fluctuations" around the Kondo temperature. The possible contributions of spin-orbit coupling and Jahn-Teller effects to impurity electronic structure are discussed, with detailed examples of how the former effect can lead to the quenching of the impurity magnetic moment below the Kondo temperature. The Anderson-model Hamiltonian, including the electron-electron interaction term U, has been reformulated to account for the large bonding-antibonding interaction and much reduced exchange splitting of the impurity-spin orbitals, and a parametrization of a "$J\vec{S}\cdot\vec{s}$" antiferromagnetic exchange Hamiltonian is suggested by the cluster electronic structure. A relationship between the concept of "cluster renormalization" and the renormalization-group method of attacking the Kondo problem is suggested, and a computational procedure for determining the effects of successive surrounding shells of atoms on the impurity, analogous to that of the renormalization-group method, is demonstrated for a 43-atom cluster. Finally, the extension of cluster molecular-orbital studies to impurity-impurity interactions, to transition-metal impurities in aluminum, where permanent local magnetic moments do not occur, to Fe impurities in palladium, where "giant magnetic moments" are observed, and to rare-earth impurities in metals is discussed.

I. INTRODUCTION

Much experimental and theoretical research has been directed to the problem of elucidating the fundamental nature of local magnetic moments associated with transition-metal impurities alloyed in nonmagnetic metals such as copper, especially in regard to the non-Curie-Weiss dependence of the magnetic susceptibility below the Kondo temperature.[1-3] Two rather different theoretical descriptions of such magnetic impurities have been proposed: (i) the virtual-impurity-state or scattering-resonance model of Friedel,[4] Anderson,[5] and Wolff,[6] and (ii) the impurity-ion "crystal-field" model of Schrieffer[7] and Hirst.[8] Two equally extreme points of view have been advanced to explain the collapse of Curie-Weiss behavior below the Kondo temperature, namely, (a) the Kondo "compensation-cloud" concept of a low-temperature many-body singlet state arising from the anti-

ferromagnetic coupling of the transition-metal impurity d-electron spin with the s-like conduction-electron spin of the host metal,[9] and (b) the concept of localized spin fluctuations (the LSF model),[3] which regards the impurity as nonmagnetic at $T=0\,^{\circ}\mathrm{K}$ and which therefore requires no extra spin correlations with the conduction electrons. Both of the latter theories have also been used as a starting point for explaining the low-temperature electrical resistance minimum associated with the Kondo effect.[1-3,10] Recent experimental studies of Kondo systems such as Fe and Mn impurities in copper, including the neutron-diffraction work of Shull and co-workers[11] and nuclear-magnetic-resonance (NMR) measurements of Slichter and co-workers,[12] have led to somewhat divergent viewpoints about the relative efficacies of these theoretical models. Such experimental studies and the recent application of renormalization-group theory[13] to the Kondo problem have catalyzed new interest in the problem of magnetic impurities in metals.

In this paper, we present a new theoretical model for local magnetic moments associated with transition-metal impurities alloyed in copper, based on self-consistent-field $X\alpha$ scattered-wave (SCF-$X\alpha$-SW) molecular-orbital studies[14] of 19-atom clusters representing the local crystalline environment of the impurities up to second-nearest neighbors, and we discuss the implications of this model on the understanding of the Kondo effect. In Sec. II of the paper, we briefly review the SCF-$X\alpha$-SW cluster molecular-orbital method and its recent applications to metal clusters, coordination complexes, and the impurity problem. Section III is devoted to a detailed comparison of the electronic structure of a 19-atom $CuCu_{12}Cu_6$ cluster representing the local molecular environment of pure crystalline copper with the band structure of the crystal. In Sec. IV, we substitute various transition-metal impurities (e.g., Ni, Fe, Mn, and V) for the central atom of the $CuCu_{12}Cu_6$ cluster as models for the isolated impurities alloyed in crystalline copper. These clusters yield manifolds of molecular-orbital energy levels corresponding to the copper "d band," bracketed by impurity dsp-hybrid-orbital energy levels that are bonding with respect to the bottom of the copper d band and antibonding with respect to the top of the d band. The latter cluster orbitals, in conjunction with Hund's rules, (i) are discrete analogs of the Friedel-Anderson virtual impurity states, (ii) satisfy a "sum rule" analogous to the Friedel sum rule, (iii) have spin occupancies and polarization in accord with measured magnetic moments, (iv) are consistent with measured trends of residual electrical resistivity, and (v) describe the "renormalizing" effects of the crystalline environment on the transition-metal impurity atom. These results have the striking implication that local coordination chemical bonding dominates the interaction of the transition-metal impurity with its crystalline environment, yielding a large splitting (~4–4.5 eV) between bonding and antibonding impurity dsp-hybrid molecular-orbital energy levels and a spin splitting (~0.2–0.6 eV) of the highest occupied antibonding dsp hybrid orbitals (the Friedel-Anderson-like impurity states) that is an order of magnitude smaller than the values assumed in previous theoretical models (e.g., the Anderson model[5]). It is further shown in Sec. IV that the near-degeneracy of the latter spin orbitals (for Fe and Mn impurities) with cluster molecular-orbital analogs of the conduction-band eigenstates of crystalline copper near the Fermi energy implies that the "spin-compensation cloud" often associated with the Kondo effect is considerably smaller in magnetization and more spatially localized around the impurity than assumed in previous formal theories. This degeneracy of spin orbitals also provides, in conjunction with the SCF-$X\alpha$ transition-state concept,[14,15] a discrete orbital basis for discussing the onset of "localized spin fluctuations" around the Kondo temperature. The possible contributions of Jahn-Teller effects to the impurity electronic structure are also discussed in Sec. IV. In Sec. V, the Anderson Hamiltonian,[5] including the electron-electron interaction term U, is reformulated to account for the large bonding-antibonding interaction and much reduced exchange splitting of the impurity spin orbitals, and a parametrization of a "$J\vec{S}\cdot\vec{s}$" antiferromagnetic exchange Hamiltonian[1,2] is suggested by the cluster electronic structures. Section VI is devoted to a demonstration of how spin-orbit coupling can lead to non-Curie-Weiss dependence and quenching of the impurity magnetic moment below the Kondo temperature. In Sec. VII, a relationship between the concept of "cluster renormalization" and the renormalization-group method[13] of attacking the Kondo problem is suggested, and a computational procedure for determining the effects of successive surrounding shells of atoms on the impurity, analogous to that of the renormalization-group method, is demonstrated for a 43-atom cluster. Finally, Sec. VIII is a discussion of the extension of cluster molecular-orbital studies to impurity-impurity interactions and to other dilute transition-metal alloys, including transition-metal impurities in aluminum, where permanent local magnetic moments do not occur, to Fe impurities in palladium, where "giant magnetic moments" are observed, and to rare-earth impurities in metals.

II. THE SCF-$X\alpha$-SW CLUSTER MOLECULAR-ORBITAL METHOD

The SCF-$X\alpha$-SW cluster molecular-orbital method[14] is based on the combined use of Slater's[15] $X\alpha$ density-functional approximation to exchange and correlation and the multiple-scattered-wave method[16] of solving the self-consistent-field Schrödinger equation. Details of the formalism and computational procedure are described in Refs. 14–16, and recent applications to a wide range of molecules and solids are reviewed in Ref. 17.

Most directly pertinent to the theoretical models presented in this paper are recent SCF-$X\alpha$-SW molecular-orbital studies of Cu, Ni, Pd, and Pt clusters containing up to 13 atoms, as reported in Refs. 18–20. One is struck by the similarities, rather than the differences, between the electronic structures of the clusters and those of the corresponding bulk metals. For example, the manifolds of orbital energy eigenvalues for 13-atom clusters having the cubo-octahedral nearest-neighbor coordination characteristic of the fcc lattice exhibit all the principal features of the bulk band structures, e.g., overlap of the "d band" by the "s,p band," a sharp peak in the density of states around the Fermi energy for the Ni_{13}, Pd_{13}, and Pt_{13} clusters, increasing bandwidth through this series, and magnetic spin polarization in the case of Ni_{13} (see Ref. 19). More recent SCF-$X\alpha$ studies of four- and six-atom nickel, palladium, and platinum clusters, including relativistic effects, indicate that even these small clusters exhibit most of the qualitative features of the crystalline band structure and can be utilized as a basis for understanding the nature of the interaction of hydrogen with these metals.[20] These predictions have been confirmed by spectroscopic studies of small noble- and transition-metal clusters isolated in inert matrices.[21,22]

Spin-polarized SCF-$X\alpha$-SW molecular-orbital studies have also been carried out for elemental Fe clusters ranging in size from 4 to 15 atoms.[23] Results for 9- and 15-atom clusters representing the local molecular environment of bcc crystalline α-iron up to second-nearest neighbors also show remarkable similarities to the electronic band structure of ferromagnetic α-iron, including: (i) exchange splitting and widths of the cluster d-orbital manifolds, particularly those for Fe_{15}, which are comparable with the values for bulk ferromagnetic iron, (ii) cluster densities of states that exhibit a pronounced two-peak structure which is primarily a consequence of the exchange splitting, consistent with the density of states of bulk ferromagnetic iron, (iii) average paramagnetic magneton numbers per atom of 2.9 and 2.5 for Fe_9 and Fe_{15}, respectively, approaching the 2.2 value for ferromagnetic crystalline α-iron, (iv) a partial-wave decomposition of cluster spin orbitals, which indicates that the contribution of the $4s$-like component to spin polarization, although relatively small in magnitude, is opposite in direction (antiparallel) to the contribution of the dominant $3d$-like component, in good agreement with magnetic form factors derived from neutron-diffraction data, and (v) a somewhat greater spin density concentrated in the cluster molecular orbitals of $e_g(d_{z^2}, d_{x^2-y^2})$ symmetry than in the $t_{2g}(d_{xy}, d_{yz}, d_{xz})$ orbitals, thereby providing a local model for the concentration of spin density along the [100] direction (the direction of easy magnetization) in crystalline α-iron, as deduced from neutron-diffraction measurements. Finally, these spin-polarized cluster molecular-orbital models have been used as a basis for describing the "spin clusters" observed in neutron-diffraction studies of crystalline α-iron above the Curie temperature.[23]

While a small noble- or transition-metal cluster does indeed exhibit most of the characteristics of the crystal band structure, the molecular boundary conditions and the fact that most of the atoms of the cluster are effectively coordinatively unsaturated "surface" atoms lead to some important additional features of the electronic structure.[19] These include the appearance of localized orbitals split off in energy from the top and bottom of the cluster d-orbital manifold, which can be interpreted as the cluster analogs of the "surface states" split off from the bulk d band for an extended crystalline surface. The surface-like orbitals can easily be distinguished from the bulk-like orbitals by virtue of the cluster molecular-orbital symmetries and charge distributions (see Fig. 15 of Ref. 19). Therefore, the electronic structures of such clusters can be used as analogs of both the bulk and surface electronic structures of the corresponding crystalline metals, as well as models for small metallic clusters of catalytic importance.[19] To test the effects of the molecular boundary conditions on a small metal cluster, SCF-$X\alpha$-SW molecular-orbital calculations have also been carried out for a bcc Fe_9 cluster where the boundary conditions have been modified to simulate the "embedding" of the cluster in the extended bcc crystalline environment.[23] Although the quantitative correspondence between the cluster electronic structure and crystal band structure is somewhat improved, e.g., through an effective increase of the cluster d-band width, the main conclusions concerning the relationships between cluster and crystal electronic structures given above, including magnetic properties, are unaltered.

Concurrent with these studies, Messmer and

Salahub[24] have carried out SCF-$X\alpha$-SW calculations for aluminum clusters (and oxygen chemisorption thereon) containing up to 43 atoms. The results indicate that 25 atoms are sufficient to yield the detailed structure and 92% of the bandwidth of the electronic density of states of crystalline aluminum, as measured by x-ray and photoelectron emission spectra. Increasing the cluster size to 43 atoms yields 99% of the crystalline bandwidth. These studies are perhaps the most definitive test of the "real-space" cluster representation of solids and surfaces made thus far, since aluminum is traditionally viewed as a highly delocalized nearly-free-electron metal for which the conventional "$\vec{k}$-space" representation of solid-state physics is most appropriate. More recently, Messmer, Salahub, and Davenport[25] have used Davenport's[26] procedure for calculating photoionization cross sections, based on the extension of the SCF-$X\alpha$-SW method to continuum final states developed by Dill and Dehmer,[27] to calculate the angular dependence of photoemission for oxygen chemisorbed on an aluminum cluster representing the (100) surface.

In using cluster molecular spin orbitals to represent the local electronic structures and magnetic moments of transition-metal impurities alloyed in crystalline metals such as coppper (see Sec. IV), we are concerned essentially with the spin-polarized electronic structure of a transition-metal coordination complex in which the surrounding atoms of the host metal lattice can be viewed as "ligands" of the complex. It is important, therefore, to establish that the SCF-$X\alpha$-SW method is also capable of accurately describing the electronic structures, chemical bonding, and magnetic properties of well-defined transition-metal coordination complexes of inorganic and organometallic chemistry.[28,29] Such results have indeed been obtained for a wide variety of transition-metal complexes,[17] ranging from inorganic systems as simple as MnO_4^- (the permanganate ion)[30] to organometallic systems as large as the active centers of iron-sulfur proteins (ferredoxin),[31] hemoglobin,[32] and copper porphine.[33] The example of ferredoxin is particularly interesting in relation to the main topic of this paper, because in its oxidized electronic state $[Fe_4S_4(SR)_4]^{2-}$ (R = organic group), it exhibits the "Kondo-like" property that its Curie-Weiss paramagnetism is quenched below room temperature. The SCF-$X\alpha$-SW studies of this system[31] indicate that this property is a result of the low-temperature spin pairing of very closely spaced molecular orbitals split in energy by the Jahn-Teller effect, a conclusion that is further supported by an observed (Jahn-Teller) distortion of the otherwise perfect cubic tetrairon-tetrasulfur geometry at low temperature. In the examples of hemoglobin[32] and copper porphine,[33] electric and magnetic hyperfine parameters have been calculated directly from the SCF-$X\alpha$-SW molecular-orbital wave functions, yielding results in good agreement with experiment. Since an accurate description of the interaction of the transition-metal sites with their molecular environments is essential to the elucidation of the properties of these systems, the above-described results give one confidence that the SCF-$X\alpha$-SW cluster molecular-orbital method is also a reasonable theoretical approach to the local interaction of magnetic transition-metal impurities with metallic hosts.

It should be pointed out that cluster molecular-orbital models of impurity states and alloy electronic structure are not a new idea. For example, Messmer and Watkins[34] were the first to use both semiempirical and SCF-$X\alpha$-SW molecular-orbital methods to describe impurity and vacancy states in diamond, Hemstreet[35] has recently applied the SCF-$X\alpha$-SW technique to transition-metal impurities in silicon, and Ellis and coworkers[36] have used a Hartree-Fock-Slater discrete-variational cluster approach in studies of LiAl alloy electronic structure. What is novel in the present work is the utilization of cluster molecular orbitals as the basis for a new theoretical model of local magnetic moments and the Kondo effect.

Finally, we point out that a number of valuable theoretical approaches to the electronic structure of dilute alloys have previously been developed, ranging from the aforementioned Friedel-Anderson[4,5] concept of the virtual impurity state to the coherent-potential and average-t-matrix approximations (CPA and ATA), the latter having the virtue of working within the framework of conventional band-structure theory and being applicable to alloys of any composition as well as the dilute limit.[37] The CPA method has also been applied to metallic alloys, e.g., the CuNi system, within the framework of cluster multiple-scattering theory,[38] utilizing Lloyd's formula[39] for the density of states associated with a set of nonoverlapping spherically symmetric scattering centers. The latter approach has the advantages of computational simplicity and direct contact with the crystalline density of states. However, it has the disadvantage of not being fully self-consistent, therefore failing to describe properly the effects of charge transfer and covalency between alloy constituents, and not leading to information about individual cluster eigenstates. As we will attempt to show in this paper, a knowledge of individual cluster molecular-orbital eigenstates is useful for elucidating

certain features of local alloy electronic structure and, when spin polarization is taken into account, provides a basis for describing local magnetic moments.

III. COMPARISON OF THE ELECTRONIC STRUCTURE OF A Cu_{19} CLUSTER WITH THE BAND STRUCTURE OF CRYSTALLINE COPPER

In order to represent more accurately the local molecular environment of transition-metal impurities alloyed in crystalline copper (see Sec. IV), we have extended SCF-$X\alpha$-SW calculations, originally restricted to the 13-atom cubo-octahedral cluster having the nearest-neighbor coordination of fcc crystalline copper,[19] to a 19-atom cluster ($CuCu_{12}Cu_6$) that includes an extra six-atom shell of second-nearest neighbors. Although no special boundary conditions to simulate the further "embedding" of the Cu_{19} cluster in an infinite crystal lattice have been imposed in these studies, recent SCF-$X\alpha$-SW studies of $Fe_9(FeFe_8)$ and $Fe_{15}(FeFe_8Fe_6)$ clusters,[23] representing the local atomic arrangement up to second-nearest neighbors in bcc crystalline α-iron, suggest that such boundary conditions do not alter the main conclusions about the relationship of cluster electronic structure and magnetic spin polarization to the corresponding bulk properties. Furthermore, because we are primarily interested in the *differences* between the electronic structure of an elemental $CuCu_{12}Cu_6$ cluster and that of an $MCu_{12}Cu_6$ cluster when transition-metal impurities (M = Ni, Fe, Mn, V, etc.) are systematically substituted for the central Cu atom, it is safe to assume that the effects of the cluster boundary conditions and other computational parameters are reasonably constant through the series.

The SCF-$X\alpha$-SW calculations were implemented for the 19-atom cluster in the same fashion as reported for the Cu_{13} cluster in Ref. 19, including the choices of atomic-sphere radii and $X\alpha$ exchange-correlation parameter. The computations were carried out on an IBM 370/168 computer and required 15 iterations, at approximately 4 min per iteration, to converge to self-consistency. In Fig. 1, we display the resulting cluster molecular-orbital energy eigenvalues. Those orbitals that have significant contributions from the central Cu atom, and therefore which are most likely to be perturbed when a transition-metal impurity is substituted for that atom, are labeled according to the irreducible representations ($a_{1g}, t_{1u}, e_g, t_{2g}$) of the cluster ($O_h$) point group and in terms of the principal partial-wave (s,p,d) components in the atomic spheres. Also indicated are the occupancies and degeneracies of the highest occupied and

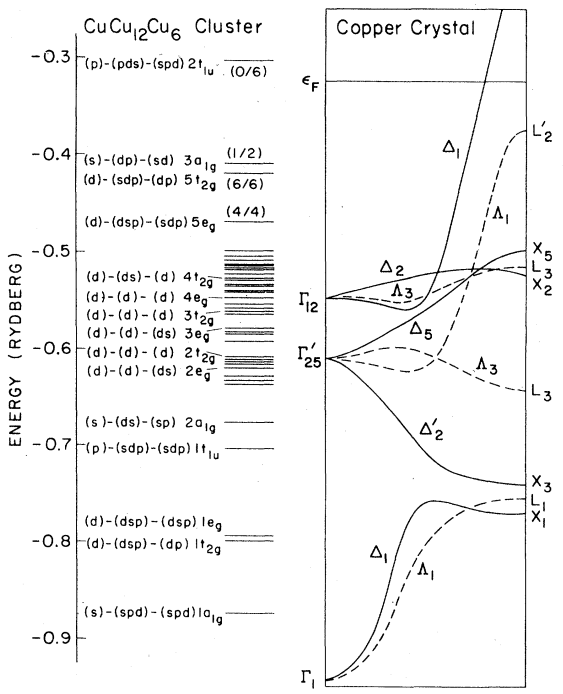

FIG. 1. SCF-$X\alpha$ molecular-orbital energy levels of a $CuCu_{12}Cu_6$ cluster representing the local environment up to second-nearest neighbors in crystalline copper. The most important levels are labeled according to the irreducible representations of the O_h point group and in terms of the principal partial-wave components on the central, nearest-neighbor, and second-nearest-neighbor Cu atoms. The orbital occupancies (degeneracies) are indicated for the three highest occupied and lowest unoccupied cluster orbitals, and these orbital occupancies satisfy a cluster "sum rule" leading to a "renormalized" $(3d)^{10}(4s)^1$-like configuration on the central Cu atom (see text). The energy-band profiles for crystalline copper, plotted along two principal symmetry directions of the Brillouin zone, are shown for comparison.

lowest unoccupied cluster orbitals. The spatial distribution of electrons and partial-wave decomposition of the highest occupied orbitals of the $CuCu_{12}Cu_6$ cluster are tabulated in Tables I(a) and II(a), respectively. Those cluster energy levels that are not labeled in Fig. 1 belong to orbitals which are nonbonding between the central atom and neighboring atoms and which therefore should be least perturbed by the substitution of transition-metal impurity atoms for the central Cu atom. Most of these orbitals transform according to the a_{1u}, a_{2g}, a_{2u}, e_u, t_{1g}, and t_{2u} irreducible representations of the O_h point group and are largely localized on the 12-atom shell of nearest neighbors or outermost six-atom shell of second-nearest neighbors in the $CuCu_{12}Cu_6$ cluster.

TABLE I. Spatial distribution of electrons (normalized to unity) in molecular orbitals of: (a) $CuCu_{12}Cu_6$, (b) $NiCu_{12}Cu_6$, (c) $FeCu_{12}Cu_6$, and (d) $VCu_{12}Cu_6$ clusters. Cu is the central copper sphere. Ni is the central nickel sphere. Fe is the central iron sphere. V is the central vanadium sphere. Cu 1 is the nearest-neighbor copper sphere. Cu 2 is the second-nearest-neighbor copper sphere. Int: intersphere region. Out: outersphere region.

(a)	Cu	Cu 1	Cu 2	Int	Out
$3a_{1g}$	1.025×10^{-1}	3.026×10^{-2}	2.846×10^{-2}	3.145×10^{-1}	4.907×10^{-2}
$5t_{2g}$	1.167×10^{-2}	2.838×10^{-2}	3.537×10^{-2}	4.020×10^{-1}	3.351×10^{-2}
$5e_g$	1.138×10^{-2}	4.107×10^{-2}	3.617×10^{-2}	2.519×10^{-1}	2.695×10^{-2}
$4t_{2g}$	2.166×10^{-2}	2.462×10^{-2}	1.040×10^{-1}	5.666×10^{-2}	2.201×10^{-3}
$4e_g$	1.456×10^{-2}	6.588×10^{-2}	2.588×10^{-2}	3.810×10^{-2}	1.571×10^{-3}
(b)	Ni	Cu 1	Cu 2	Int	Out
$3a_{1g}$	1.073×10^{-1}	2.650×10^{-2}	2.787×10^{-2}	3.488×10^{-1}	5.870×10^{-2}
$5t_{2g}$	1.033×10^{-1}	2.659×10^{-2}	2.481×10^{-2}	3.944×10^{-1}	3.433×10^{-2}
$5e_g$	2.305×10^{-1}	2.490×10^{-2}	3.193×10^{-2}	2.511×10^{-1}	2.808×10^{-2}
$4t_{2g}$	3.172×10^{-1}	2.532×10^{-2}	5.974×10^{-2}	1.907×10^{-2}	1.403×10^{-3}
$4e_g$	1.638×10^{-1}	2.725×10^{-2}	8.171×10^{-2}	1.690×10^{-2}	2.073×10^{-3}
(c)	Fe	Cu 1	Cu 2	Int	Out
$3a_{1g}$	8.925×10^{-2}	2.380×10^{-2}	2.824×10^{-2}	3.810×10^{-1}	7.481×10^{-2}
$5t_{2g}$	3.786×10^{-1}	1.924×10^{-2}	1.031×10^{-2}	3.120×10^{-1}	1.660×10^{-2}
$5e_g$	6.230×10^{-1}	1.297×10^{-2}	1.436×10^{-2}	1.259×10^{-1}	9.292×10^{-3}
$4t_{2g}$	2.873×10^{-1}	2.768×10^{-2}	4.280×10^{-2}	1.194×10^{-1}	4.338×10^{-3}
$4e_g$	1.077×10^{-1}	4.369×10^{-2}	3.440×10^{-2}	1.531×10^{-1}	8.568×10^{-3}
(d)	V	Cu 1	Cu 2	Int	Out
$3a_{1g}$	7.287×10^{-2}	2.147×10^{-2}	2.856×10^{-2}	4.107×10^{-1}	8.738×10^{-2}
$5t_{2g}$	5.163×10^{-1}	1.575×10^{-2}	4.244×10^{-3}	2.547×10^{-1}	1.451×10^{-2}
$5e_g$	6.704×10^{-1}	1.088×10^{-2}	1.105×10^{-2}	1.234×10^{-1}	9.414×10^{-3}
$4t_{2g}$	1.330×10^{-1}	3.012×10^{-2}	4.795×10^{-2}	2.099×10^{-1}	8.116×10^{-3}
$4e_g$	5.182×10^{-2}	4.351×10^{-2}	3.689×10^{-2}	1.941×10^{-1}	1.062×10^{-2}

Although it is generally improper to compare cluster molecular-orbital eigenstates with individual Bloch eigenstates of the crystal band structure, for which the reciprocal-space wave vector $\vec{k}$ is a good quantum number, it is possible, in principle, to construct linear combinations of degenerate Bloch states of different $\vec{k}$ (the so-called "star" of the wave vector) that transform according to the irreducible representations of the cluster (O_h) point group.[40] Bloch states corresponding to $\vec{k}=0$ (the Γ point of the Brillouin zone) automatically transform according to the irreducible representations of the O_h group. In these respects, one is justified in comparing the SCF-$X\alpha$ orbital energy levels of the Cu_{19} cluster with energy bands of the type originally calculated for crystalline copper by Segall[41] and Burdick,[42] as illustrated in Fig. 1 for band profiles along the [100] ($\Gamma\Delta X$) and [111] ($\Gamma\Lambda L$) directions of the Brillouin zone. This type of comparison complements the ones for cluster and crystal densities of states carried out in Refs. 19 and 24, and helps to clarify the effects of transition-metal impurities on the copper band structure.

Thus the $1a_{1g}$ level of the Cu_{19} cluster, belonging to a predominantly s-like molecular orbital, corresponds approximately to the Γ_1 ($\vec{k}=0$) s-band minimum of crystalline copper. The $1t_{2g}$ and $1e_g$ orbitals, respectively, are spatially localized degenerate bonding combinations of (d_{xy}, d_{yz}, d_{xz}) and $(d_{z^2}, d_{x^2-y^2})$ orbitals on the central Cu atom with dsp hybrid orbitals on the neighboring atoms. Although they have no simple one-to-one correspondence with the Bloch band eigenstates of crystal-

TABLE II. Partial-wave decomposition (in percentage) of molecular orbitals of: (a) $CuCu_{12}Cu_6$, (b) $NiCu_{12}Cu_6$, (c) $FeCu_{12}Cu_6$, and (d) $VCu_{12}Cu_6$ clusters. Cu is the central copper sphere. Ni is the central nickel sphere. Fe is the central iron sphere. V is the central vanadium sphere. Cu 1 is the nearest-neighbor atomic sphere. Cu 2 is the second-nearest-neighbor copper sphere.

	Cu			Cu 1			Cu 2		
(a)	$l=0$	$l=1$	$l=2$	$l=0$	$l=1$	$l=2$	$l=0$	$l=1$	$l=2$
$3a_{1g}$	100	0	0	4	26	70	37	2	61
$5t_{2g}$	0	0	100	57	20	23	0	19	81
$5e_g$	0	0	100	16	16	68	74	1	25
$4t_{2g}$	0	0	100	7	2	91	0	0	100
$4e_g$	0	0	100	0	1	99	1	0	99
	Ni			Cu 1			Cu 2		
(b)	$l=0$	$l=1$	$l=2$	$l=0$	$l=1$	$l=2$	$l=0$	$l=1$	$l=2$
$3a_{1g}$	100	0	0	3	38	59	47	2	51
$5t_{2g}$	0	0	100	62	23	15	0	26	74
$5e_g$	0	0	100	25	26	49	92	2	6
$4t_{2g}$	0	0	100	0	2	98	0	0	100
$4e_g$	0	0	100	2	0	98	0	0	100
	Fe			Cu 1			Cu 2		
(c)	$l=0$	$l=1$	$l=2$	$l=0$	$l=1$	$l=2$	$l=0$	$l=1$	$l=2$
$3a_{1g}$	100	0	0	0	49	51	43	4	53
$5t_{2g}$	0	0	100	48	27	25	0	45	55
$5e_g$	0	0	100	13	19	68	90	1	9
$4t_{2g}$	0	0	100	21	10	69	0	5	95
$4e_g$	0	0	100	11	10	79	43	1	56
	V			Cu 1			Cu 2		
(d)	$l=0$	$l=1$	$l=2$	$l=0$	$l=1$	$l=2$	$l=0$	$l=1$	$l=2$
$3a_{1g}$	100	0	0	0	63	37	47	6	47
$5t_{2g}$	0	0	100	25	36	39	0	76	24
$5e_g$	0	0	100	4	21	75	87	0	13
$4t_{2g}$	0	0	100	36	14	50	0	8	92
$4e_g$	0	0	100	14	14	72	54	2	44

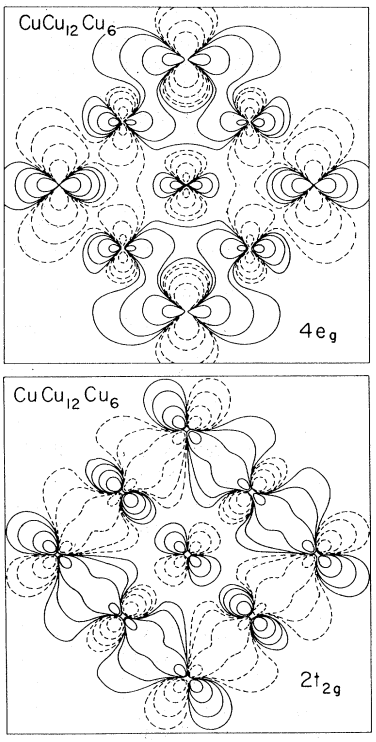

FIG. 2. Contour maps of the $2t_{2g}$ and $4e_g$ molecular-orbital wave functions for a $CuCu_{12}Cu_6$ cluster plotted in the y-z plane passing through the central atom, four nearest-neighbor atoms, and four second-nearest-neighbor atoms (see top half of Fig. 4). Solid and dashed contours represent opposite signs of wave function. The $2t_{2g}$ and $4e_g$ orbitals are discrete cluster analogs of the $\Gamma_{25'}$ and Γ_{12} d-band eigenstates, respectively, for crystalline copper.

line copper, linear combinations of degenerate band eigenstates for $\vec{k} \neq 0$ (e.g., Λ_1 and Δ_1) that transform like the $1t_{2g}$ and $1e_g$ cluster orbitals, respectively, can be found near the bottom of the d band. The $1t_{1u}$ and $2a_{1g}$ cluster levels belong to dsp-hybrid orbitals primarily localized on the 12-atom shell of nearest neighbors and correspond approximately to combinations of crystal eigenstates (e.g., $\Delta_1 X_1$ and $\Delta_2' X_3$) at the botton of the d band. The manifold of densely spaced levels between the energies, -0.65 and -0.5 Ry, is the cluster analog of the crystal d band. The $2t_{2g}$ and $4e_g$ cluster levels are isomorphic to the Γ_{25}' ($\vec{k}=0$) and Γ_{12} ($\vec{k}=0$) band eigenstates, respectively, and belong to orbitals that have (d_{xy}, d_{yz}, d_{xz}) and $(d_{z^2}, d_{x^2-y^2})$ character, respectively, around the central Cu atom, as revealed by the orbital wave-function contours in Fig. 2 mapped in a plane passing through the central atom, four nearest neighbors, and four second-nearest neighbors. The coordinate system and atomic sphere radii in the y-z plane used to generate such contour maps are shown in Fig. 4. The solid and dashed contours represent opposite signs of the orbital wave function. The $4e_g$ orbital, for example, is largely nonbonding between the central atomic d_{z^2} orbital and nearest-neighbor d orbitals, whereas it is formally bonding between the central d_{z^2} orbital and second-nearest neighbor d orbitals. The $2e_g$, $3e_g$, $3t_{2g}$, and $4t_{2g}$ levels in the cluster d-orbital manifold have a rough equivalence to mixed bonding and antibonding combinations of degenerate crystal d-band eigenstates for $\vec{k} \neq 0$. The unlabeled cluster levels between the energies -0.525 and -0.5 Ry correspond to combinations of crystal

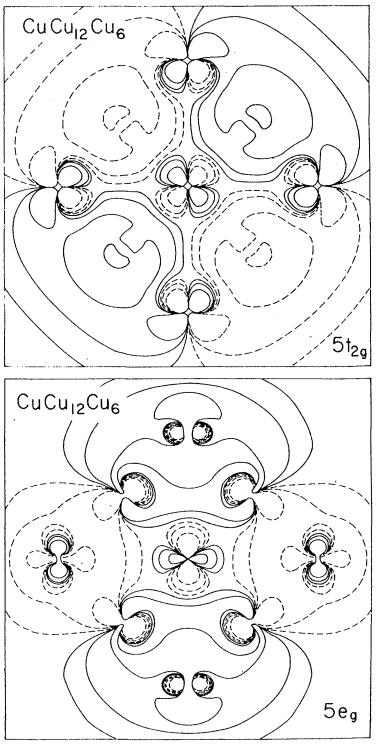

FIG. 3. Contour maps of the $5e_g$ and $5t_{2g}$ molecular-orbital wave functions for a $CuCu_{12}Cu_6$ cluster plotted in the y-z plane shown in the top half of Fig. 4. These orbitals, which are antibonding between the central atom and surrounding atoms, are discrete cluster analogs of dsp-hybrid energy-band eigenstates for crystalline copper between the top of the d band and Fermi energy (see text).

eigenstates (e.g., $\Delta_2 X_2$, $\Lambda_3 L_3$, and $\Delta_5 X_5$) at the top of the d band.

The $5e_g$, $5t_{2g}$, and $3a_{1g}$ levels are the highest occupied eigenstates of the Cu_{19} cluster. The occupancies and degeneracies of these molecular orbitals are indicated in Fig. 1. The spatial distribution of electrons and partial-wave decomposition of these orbitals are tabulated in Tables I(a) and II(a). These orbitals deserve special consideration, because, along with the $4e_g$ and $4t_{2g}$ eigenstates near the top of the d band, they are most strongly perturbed and evolve into cluster analogs of the Friedel-Anderson virtual impurity states[4,5] when first-row transition elements are substituted for the central Cu atom (see Sec. IV). Thus they are key orbitals in a cluster model for local magnetic moments and residual resistivity in dilute transition-metal-copper alloys. The $5e_g$ cluster molecular orbital, mapped in Fig. 3, is a spatially delocalized antibonding composite of $(d_{z^2}, d_{x^2-y^2})$ orbital character on the central Cu atom and dsp-hybrid orbital character on the nearest and second-nearest neighboring Cu atoms. The $5e_g$ cluster eigenstate is roughly equivalent to a combination of crystal eigenstates (e.g., Δ_1) where the s, p-like "conduction band" has just emerged from the top of the d band (see Fig. 1). Similarly, the $5t_{2g}$ cluster orbital, also mapped in Fig. 3, is a spatially delocalized antibonding composite of (d_{xy}, d_{yz}, d_{xz}) orbital character on the central Cu atom, sdp-hybrid-orbital character on the nearest-neighboring Cu atoms, and dp-hybrid-orbital character on the second-nearest neighbors. This orbital corresponds approximately to a combination of hybrid conduction-band eigenstates (e.g., Λ_1) of crystalline copper just below the Fermi energy. The highest occupied Cu_{19} cluster molecular orbital, $3a_{1g}$, which is a spatially delocalized mixture of spherically-symmetric $4s$-like orbital

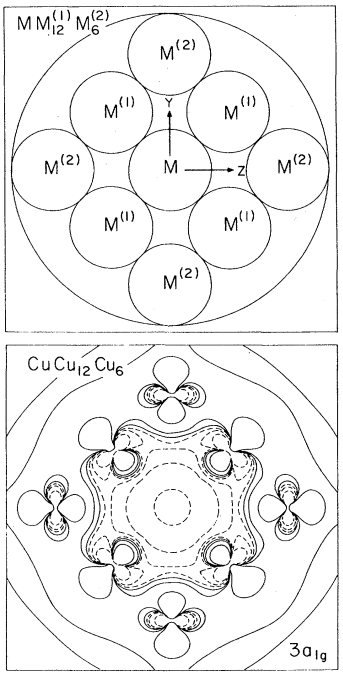

FIG. 4. Contour map of the $3a_{1g}$ molecular-orbital wave functions for a $CuCu_{12}Cu_6$ cluster plotted in a y-z plane passing through the central atom, four nearest-neighbor atoms, and four second-nearest-neighbor atoms shown in the top half of the figure. The half-occupied (1/2) $3a_{1g}$ orbital, which is antibonding between the central atom and surrounding atoms, is the discrete cluster analog of the half-filled sd-hybrid conduction band of crystalline copper around the Fermi energy, as indicated by the spherically symmetric s-like orbital character on the central atom, d-like orbital character on nearest-neighbor atoms, and sd-hybrid orbital character on the second-nearest-neighbor atoms (see text).

character on the central Cu atom with dp- and sd-hybrid-orbital character on the surrounding shells of atoms (see the orbital contour map in Fig. 4), is the counterpart of crystal conduction-band states (e.g., Δ_1) at the Fermi energy. Thus the $3a_{1g}$ orbital, which is only half occupied, defines the "Fermi energy" of the 19-atom cluster and is the discrete cluster analog of the half-filled conduction "s band" of crystalline copper. This correspondence is extremely valuable in using the cluster electronic structure to describe the coupling of transition-metal impurity spin orbitals to the conduction-band spin orbitals in connection with the Kondo problem[1-3] (see Sec. IV). Finally, the lowest unoccupied Cu_{19} cluster energy level, $2t_{1u}$, shown in Fig. 1 belongs to a highly delocalized molecular orbital that is predominantly $4p$-like on the central and nearest-neighboring Cu atoms and predominantly $4s$-like on the second-nearest neighbors. It is the cluster analog of empty crystal conduction-band eigenstates above the Fermi level.

Although the highest occupied Cu_{19} molecular orbitals, $5e_g$, $5t_{2g}$, and $3a_{1g}$, are spatially delocalized on the nearest and second-nearest shells of atoms and are cluster analogs of crystalline copper conduction-band states around the Fermi energy, they formally transform respectively like $(d_{z^2}, d_{x^2-y^2})$,[4] (d_{xy}, d_{yz}, d_{xz}),[6] and $(s)^1$ orbital configurations on the central Cu atom in analogy to the $(3d)^{10}(4s)^1$ configuration of a free Cu atom. It has been shown in Fig. 5 of Ref. 19 that a 13-atom cubo-octahedral cluster ($CuCu_{12}$) representing the nearest-neighbor environment in crystalline copper yields only one occupied molecular orbital near the Fermi energy, namely, a t_{2g} orbital containing five electrons, formally corresponding to a $(d_{xy}, d_{yz}, d_{xz})^5(d_{z^2}, d_{x^2-y^2})^0$ $(s)^0$- or $(3d)^5$ $(4s)^0$-like orbital configuration on the central atom. Thus the addition of a six-atom shell of second-nearest neighbors to the Cu_{13} cluster, resulting in a Cu_{19} ($CuCu_{12}Cu_6$) cluster, "coordinatively saturates" the central Cu atom and provides six more valence ($4s$) electrons that populate the $5e_g$, $5t_{2g}$, and $3a_{1g}$ molecular orbitals, effectively resulting in a $(d_{z^2}, d_{x^2-y^2})^4(d_{xy}, d_{yz}, d_{xz})^6$ $(s)^1$- or $(3d)^{10}(4s)^1$-like configuration on the central atom. The extra 60 $3d$ electrons provided by the six second-nearest neighbors populate extra orbitals (as compared with Cu_{13}) in the cluster d band below the $5e_g$, $5t_{2g}$, and $3a_{1g}$ levels. We can view the attainment of the neutral-atom electron configuration in the Cu_{19} cluster as the satisfying of a cluster "sum rule." This interpretation suggests that a 19-atom cubo-octahedral cluster is adequate for describing the "renormalizing" effects on the local fcc crystalline copper environment on a copper atom and, as shown in Sec. IV, on a substitutional transition-metal impurity. The concept of "cluster renormalization" is a way of interpreting the most important effects of delocalized molecular-orbital formation between the central metal atom and its surrounding shells of atoms and should not be confused with the "renormalized-atom" concept of Hodges *et al.*[43] However, there are possible conceptual and computational relationships of cluster renormalization to the "renormalization-group" method[13] of solving the Kondo problem, as discussed in Sec. VII.

IV. CLUSTER MOLECULAR-ORBITAL MODELS OF TRANSITION-METAL IMPURITIES ALLOYED IN COPPER

A. General trends of electronic structure and the cluster sum rule

In Fig. 5, we display the molecular-orbital energy eigenvalues, calculated by the SCF-$X\alpha$-SW method, for $NiCu_{12}Cu_6$, $FeCu_{12}Cu_6$, and $VCu_{12}Cu_6$ clusters representing the local environment (up to second-nearest neighbors) of isolated substitutional Ni, Fe, and V impurities in an otherwise perfect crystalline copper lattice. Comparing these energy levels with the $CuCu_{12}Cu_6$ levels simulating the band structure of pure crystalline copper in Fig. 1, we note the following general trends of electronic structure:

(i) The interaction of each transition-metal impurity with the surrounding copper atoms, viewed as "ligands" of a transition-metal coordination complex,[28,29] leads to molecular orbitals ($1e_g$ and $1t_{2g}$) at the bottom of the copper d band that are bonding between the transition-metal d orbitals and dsp-hybrid orbitals on the surrounding Cu atoms, and to molecular orbitals ($4e_g$ and $4t_{2g}$) near the top of the copper d band that are antibonding between the transition-metal d orbitals and nearest-neighbor Cu d orbitals. Contour maps of these orbitals are shown, for example, for the $FeCu_{12}Cu_6$ cluster in Figs. 8 and 9. However, note in Fig. 9 for the $4e_g$ eigenstate of the $FeCu_{12}Cu_6$ cluster that, while the central Fe d_{z^2}-like orbital is antibonding with respect to similar orbitals on the nearest-neighbor Cu atoms, it is bonding in relation to second-nearest neighbors.

(ii) There is significant mixing of transition-metal antibonding d-orbital character in the $5e_g$ and $5t_{2g}$ cluster eigenstates (see Fig. 5), which increases across the first-row transition series from Ni to Fe to V, as revealed by the spatially expanding $(d_{z^2}, d_{x^2-y^2})$ and (d_{xy}, d_{yg}, d_{xz}) orbital character on the central transition-metal impurity in Figs. 7, 10, and 11. These eigenstates are discrete cluster molecular-orbital analogs of the

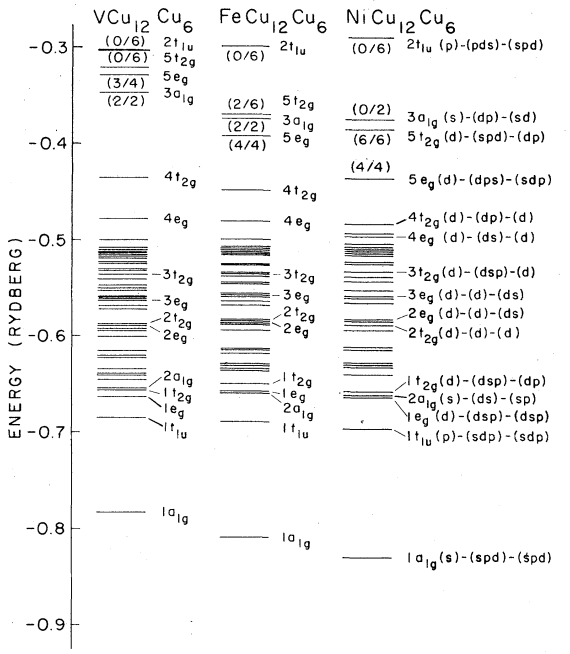

FIG. 5. SCF-$X\alpha$ molecular-orbital energy levels of clusters representing the local enviroment up to second-nearest neighbors of isolated substitutional Ni, Fe, and V impurities in crystalline copper. The most important levels are labeled according to the irreducible representations of the O_h point group and in terms of the principal partial-wave components of the central impurity atom and surrounding Cu atoms. The orbital occupancies (degeneracies) are indicated for the three highest occupied and lowest unoccupied cluster orbitals, and these orbital occupancies satisfy a cluster "sum rule" leading to a "renormalized " atomiclike configuration on the central impurity atom. The $5e_g$ and $5t_{2g}$ orbitals are discrete cluster analogs of the Friedel-Anderson impurity virtual d orbitals, split in energy and orbital degeneracy by the antibonding interaction with sd-hybrid orbitals on the surrounding atoms viewed as ligands, while the $(1e_g, 1t_{2g})$ and $(4e_g, 4t_{2g})$ pairs of levels are bonding and antibonding, respectively, with respect to the bottom and top of the d band. Note that the order of the $4e_g$ and $4t_{2g}$ levels, as well as the order of the $5e_g$ and $5t_{2g}$ levels, is the reverse of that in ligand-field theory for sixfold coordinated ligands (the second-nearest neighbors in these clusters) because the intervening 12 nearest neighbors interact directly with the central-atom d components in the $4t_{2g}$ and $5t_{2g}$ orbitals (see Figs. 6 and 7), pushing the latter to higher energies with respect to the $4e_g$ and $5e_g$ orbitals which are directed toward the second-nearest neighbors.

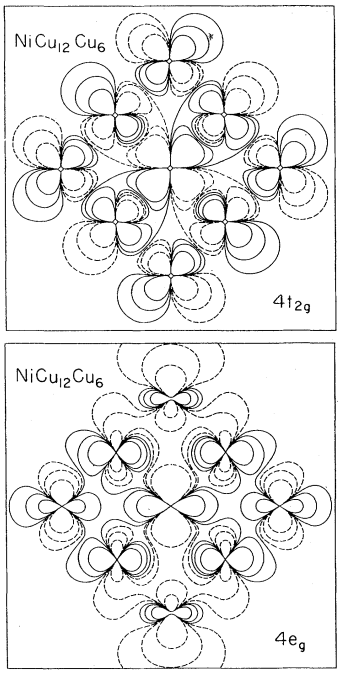

FIG. 6. Contour maps of the $4e_g$ and $4t_{2g}$ molecular-orbital wave functions for $NiCu_{12}Cu_6$ cluster plotted in the y-z plane shown in the top half of Fig. 4. The antibonding interaction between the central Ni-impurity-atom d_{z^2} and d_{yz} components of the $4e_g$ and $4t_{2g}$ orbitals, respectively, and the nearest-neighbor Cu d components is clearly visible, along with the formal bonding relation between the central Ni-impurity-atom d_{z^2} component and second-nearest-neighbor Cu d components in the $4e_g$ orbital.

Friedel-Anderson virtual impurity states,[4,5] split in energy and degeneracy by the antibonding interaction of the impurity d orbitals with the s, p, d hybrid orbitals on the surrounding Cu atoms.

(iii) The $4s$-like contribution of the transition-metal atom to the $3a_{1g}$ orbital of each impurity cluster in Fig. 5 is spatially indistinguishable from a Cu $4s$-like contribution. In Sec. III (Fig. 1), we have shown that the half-filled $3a_{1g}$ orbital of a $CuCu_{12}Cu_6$ cluster is the discrete analog of the half-filled conduction band of crystalline copper near the Fermi energy. Thus the $3a_{1g}$ orbital, when fully occupied and spin paired as indicated for $FeCu_{12}Cu_6$ and $VCu_{12}Cu_6$ in Fig. 5, describes within the framework of the cluster electronic structure the coupling of the impurity to the conduction-band eigenstates of copper.

(iv) The $5e_g(d_{z^2}, d_{x^2-y^2})$, $5t_{2g}(d_{xy}, d_{yz}, d_{xz})$, and $3a_{1g}(s)$ cluster molecular orbitals in Fig. 5, like those discussed in Sec. III for the $CuCu_{12}Cu_6$ cluster (Fig. 1), can be interpreted simplistically as "renormalized" transition-metal impurity orbitals, the occupancies of which satisfy a cluster sum rule analogous to the Friedel sum rule.[4] As indicated by the orbital occupancies in Fig. 5, the

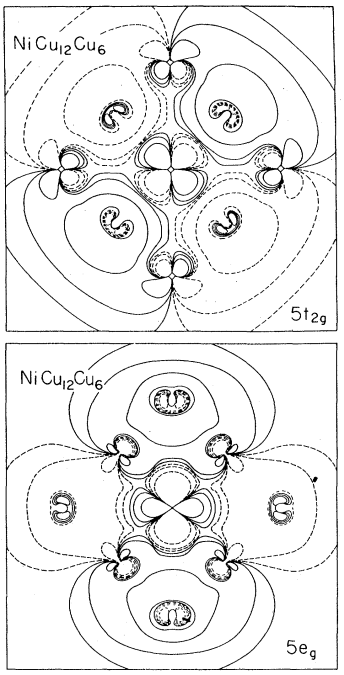

FIG. 7. Contour maps of the $5e_g$ and $5t_{2g}$ molecular-orbital wave functions for a $NiCu_{12}Cu_6$ cluster plotted in the y-z plane shown in the top half of Fig. 4. These orbitals, which are antibonding between the central Ni-impurity-atom d components and sd-hybrid components on the surrounding Cu atoms, are discrete cluster analogs of the Friedel-Anderson virtual impurity states. Note the expanded d amplitude on the central Ni impurity atom, as compared with that on the central Cu atom in the corresponding orbitals of Fig. 3.

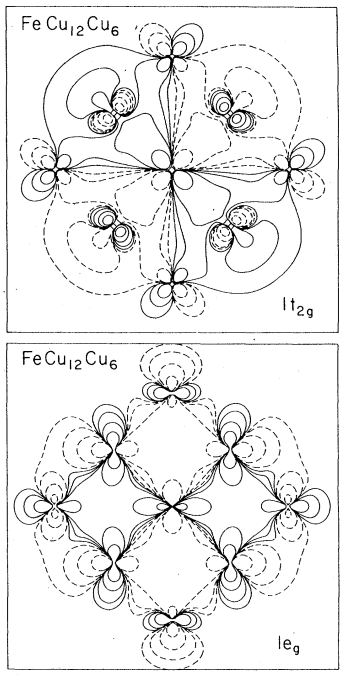

FIG. 8. Contour maps of the $1e_g$ and $1t_{2g}$ molecular-orbital wave functions for a $FeCu_{12}Cu_6$ cluster plotted in the y-z plane shown in the top half of Fig. 4. The bonding relationships between the central Fe-impurity-atom d_{z^2} and d_{yz} components of the $1e_g$ and $1t_{2g}$ orbitals, respectively, and the d-like components on the surrounding Cu atoms are clearly visible.

electron configurations of the $5e_g(d_{z^2}, d_{x^2-y^2})$, $5t_{2g}(d_{xy}, d_{yz}, d_{xz})$, and $3a_{1g}(s)$ orbitals are formally analogous to a $(3d)^{10}(4s)^0$ configuration for $NiCu_{12}Cu_6$, a $(3d)^6(4s)^2$ configuration for $FeCu_{12}Cu_6$, and a $(3d)^3(4s)^2$ configuration for $VCu_{12}Cu_6$.

(v) Other configurations attained by electron promotion between the highest occupied and lowest unoccupied cluster molecular orbitals ($3a_{1g}$, $5t_{2g}$) result in the respective "renormalized-impurity-atom" configurations $(3d)^9(4s)^1$ ($NiCu_{13}Cu_6$), $(3d)^7(4s)^1$ ($FeCu_{12}Cu_6$), and $(3d)^4(4s)^1$ ($VCu_{12}Cu_6$), which are closer in energy to the above configurations than corresponding configurational energy differences in the free atoms, as determined by the SCF-$X\alpha$ transition-state method.[14,15] This result is relevant to the onset of localized spin fluctuations discussed in Sec. IV C.

With the above general trends in mind, we now describe in somewhat more detail the use of the individual cluster electronic structures in Fig. 5 as a basis for understanding the electronic structures and magnetic properties of transition-metal impurities alloyed in copper.

B. $NiCu_{12}Cu_6$ and the concept of "cluster renormalization"

Comparing Figs. 5 through 7 with Figs. 1 through 3, we find that the most important effects of substituting a Ni impurity for the central Cu atom in a $CuCu_{12}Cu_6$ cluster are the shifting in energy of the $4e_g$ and $4t_{2g}$ eigenstates to the top of the d band and the significant mixing of Ni d-orbital character in these eigenstates and in the $5e_g$ and $5t_{2g}$ orbitals. The $4t_{2g}$ and $5e_g$ eigenstates contain the largest amount of Ni $3d$-like character and are discrete molecular-orbital precursors of the narrow Ni impurity subband that is split off in energy from the top of the Cu d band and below the Fermi energy in photoemission spectra[44,45] and ATA band-structure calculations[46] for dilute CuNi alloys. A comparison of the $5e_g$ orbital contour maps for the $NiCu_{12}Cu_6$ and $CuCu_{12}Cu_6$ clusters in Figs. 7 and 3, respectively, reveals the expanded

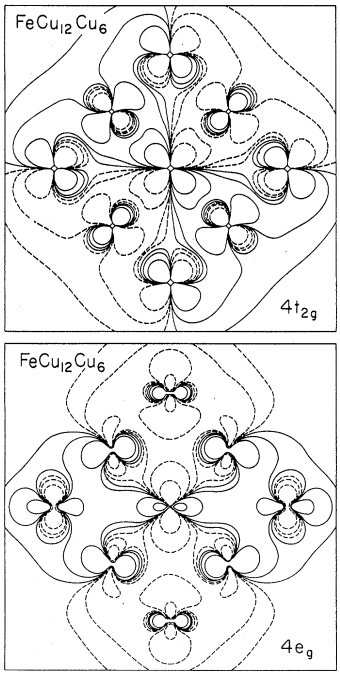

FIG. 9. Contour maps of the $4e_g$ and $4t_{2g}$ molecular-orbital wave functions for a $FeCu_{12}Cu_6$ cluster plotted in the y-z plane shown in the top half of Fig. 4. The antibonding interaction between the central Fe-impurity-atom d_{z^2} and d_{yz} components of the $4e_g$ and $4t_{2g}$ orbitals, respectively, and the nearest-neighbor Cu d components is clearly visible, along with the formal bonding relation between the central Fe-impurity-atom d_{z^2} component and second-nearest-neighbor Cu d components in the $4e_g$ orbital.

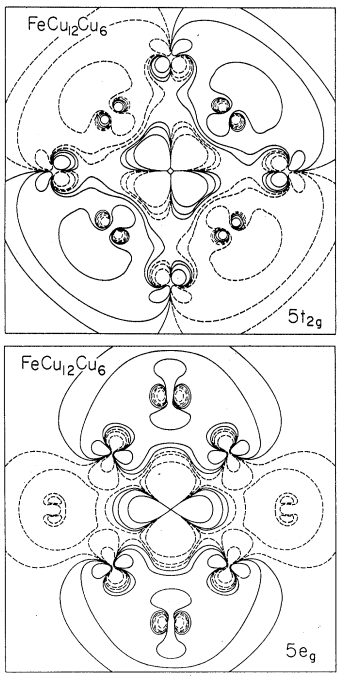

FIG. 10. Contour maps of the $5e_g$ and $5t_{2g}$ molecular-orbital wave functions for a $FeCu_{12}Cu_6$ cluster plotted in the y-z plane shown in the top half of Fig. 4. These orbitals, which are antibonding between the central Fe impurity-atom d components and sd-hybrid components on the surrounding Cu atoms, are discrete cluster analogs of the Friedel-Anderson virtual impurity states. Note the expanded d amplitude on the central Fe impurity atom as compared with that on the central Ni impurity atom in the corresponding orbitals of Fig. 7.

d_{z^2}-orbital character on the central Ni atom and its antibonding relationship to localized $3d$-like orbitals and delocalized $4s$-like orbitals on the surrounding Cu atoms. The $5e_g$-orbital of the $NiCu_{12}Cu_6$ cluster provides an excellent "real-space" representation of the initial states associated with the photoemission peak between the d band and Fermi energy of dilute CuNi alloys, and the directional character of the $5e_g$ orbital underlies the angular resolution of this photoemission peak.[45] This spatial molecular-orbital character underscores the chemical nature of the interaction of a transition-metal impurity in a copper environment, in particular, the importance of d-d interactions, and suggests that the traditional picture of the Friedel-Anderson[4,5] virtual impurity state as an atomic d orbital "resonating" in a purely s-like free-electron gas is too simplistic.

Although the ground-state electron configuration of a free Ni atom is the magnetic one, $(3d)^8(4s)^2$, the "renormalizing" effect of the surrounding Cu atoms in the $NiCu_{12}Cu_6$ cluster results in a nonmagnetic $(d_{z^2}, d_{x^2-y^2})^4(d_{xy}, d_{yz}, d_{xz})^6$ $(s)^0$- or effective $(3d)^{10}(4s)^0$-like "closed-shell" configuration of the $5e_g$, $5t_{2g}$, and $3a_{1g}$ orbitals, consistent with the nonmagnetic state of dilute nickel impurities alloyed in crystalline copper.[1,2]

C. Local magnetic moments and the Kondo problem

The perturbing effects of a substitutional Fe impurity on the $CuCu_{12}Cu_6$ cluster electronic structure are significantly more severe than in the case of Ni, as revealed by a comparison of Figs. 1 and 5. The $4e_g$ and $4t_{2g}$ orbitals of the $FeCu_{12}Cu_6$, mapped in Fig. 9, are now pushed out of the top of the copper d band, and there is a large amount of antibonding Fe $3d$-like character mixed into the $5e_g$ and $5t_{2g}$ orbitals, as shown by the greatly expanded central-atom d_{z^2}- and d_{yz}-orbital character in the respective orbital contour maps of Fig. 10.

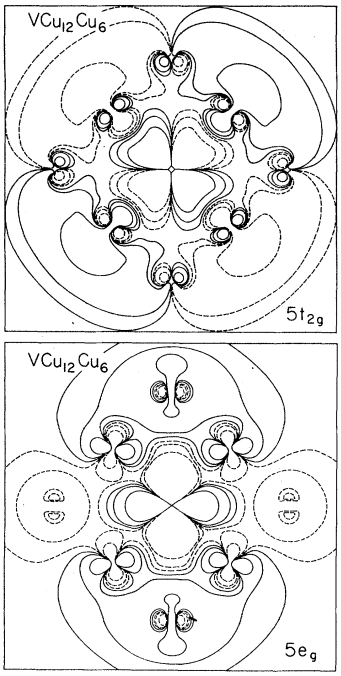

FIG. 11. Contour maps of the $5e_g$ and $5t_{2g}$ molecular-orbital wave functions for a $VCu_{12}Cu_6$ cluster plotted in the y-z plane shown in the top half of Fig. 4. These orbitals, which are antibonding between the central V impurity-atom d components and sd-hybrid components on the surrounding Cu atoms, are discrete cluster analogs of the Friedel-Anderson virtual impurity states. Note the expanded d amplitude on the central V impurity atom as compared with that on the central Fe impurity atom in the corresponding orbitals of Fig. 10.

The electron configuration of the $5e_g$, $5t_{2g}$, and $3a_{1g}$ orbitals in the $FeCu_{12}Cu_6$ cluster is $(d_{z^2}, d_{x^2-y^2})^4(d_{xy}, d_{yz}, d_{xz})^2$ $(s)^2$ or effectively like the $(3d)^6(4s)^2$ configuration of a free Fe atom. Thus, in contrast to the nonmagnetic state of the $NiCu_{12}Cu_6$ cluster, the open-d-shell configuration of the $FeCu_{12}Cu_6$ cluster allows for the possibility of magnetic spin polarization.

Aside from the issue of spin polarization, the partial occupancy (2/6) of the $5t_{2g}$ orbital of the $FeCu_{12}Cu_6$ cluster also suggests the possibility of a Jahn-Teller instability of the ideal cubic (O_h) geometry. This could lead to a lowering of the cluster symmetry and to the splitting of the sixfold degenerate t_{2g} orbital into an unoccupied fourfold degenerate orbital (e) and fully occupied twofold degenerate orbital (a), as illustrated schematically by the inset in Fig. 12. The spin-paired ground electronic configuration implied by such a Jahn-Teller effect would suggest a nonmagnetic state of the Fe impurity at 0 °K and a Curie-Weiss paramagnetic state at higher temperatures arising from thermally induced electronic excitations across the energy gap Δ_{JT}. Although we have not calculated Δ_{JT} for the $FeCu_{12}Cu_6$ cluster, both experiment and SCF-$X\alpha$-SW electronic-structure calculations for the approximately cubic $[Fe_4S_4(SR)_4]^{2-}$ cluster (R = organic group that represents the active center of the iron-sulfur protein, ferredoxin (see discussion in Sec. II) indicate that the "Kondo-like" transition from Curie-Weiss paramagnetism to the nonmagnetic state below room temperature is the result of the Jahn-Teller splitting of a partially occupied (4/6) degenerate orbital of t_2 symmetry into a fully occupied (4/4) e orbital and empty (0/2) b_2 orbital (see Fig. 1 of Ref. 31), yielding a spin-paired (singlet) ground state. A Δ_{JT} value equivalent to the Kondo temperature (~7 °K), below which Fe impurities in copper lose Curie-Weiss magnetism,[1-3] would be consistent with the *dynamic* rather than the static Jahn-Teller effect.[47] However, there is no definitive experimental evidence for Jahn-Teller effects associated with Fe impurities in copper, although they are quite common for "deep-level" impurities in semiconductors[34] and for transition-metal coordination complexes.[29]

If the orbital angular momentum of the transition-metal impurity is not fully quenched by the copper environment, then spin-orbit coupling should be competitive with or indeed act in conjunction with Jahn-Teller effects for splitting the degenerate impurity molecular-orbital energy levels.[47] Such spin-orbit splitting, under certain circumstances, can then lead to the quenching of the impurity magnetic moment at low temperature, in spite of the unpaired impurity spin, as a result of the cancellation of spin and orbital contributions to the magnetic moment. Such effects are well known to occur in transition-metal coordination complexes,[29] and in Sec. VI of this paper we will present detailed quantitative examples illustrating how spin-orbit coupling can account for the quenching of the transition-metal impurity magnetic moment below the Kondo temperature.

Neglecting Jahn-Teller and spin-orbit contributions, we can determine the magnetic spin polarization of the $FeCu_{12}Cu_6$ cluster, from first principles, by applying the spin-unrestricted version of the SCF-$X\alpha$-SW method[14-16] in conjunction with Hund's rules. This leads to different cluster molecular orbitals for "spin-up ($\uparrow$)" and "spin-down ($\downarrow$)" electrons, as shown in Fig. 12 for the three highest occupied orbitals ($5e_g$, $5t_{2g}$, $3a_{1g}$) of the $FeCu_{12}Cu_6$ cluster on a more highly resolved energy scale than in Fig. 5. The corresponding non-spin-polarized orbital energies are included for comparison. The most immediately striking

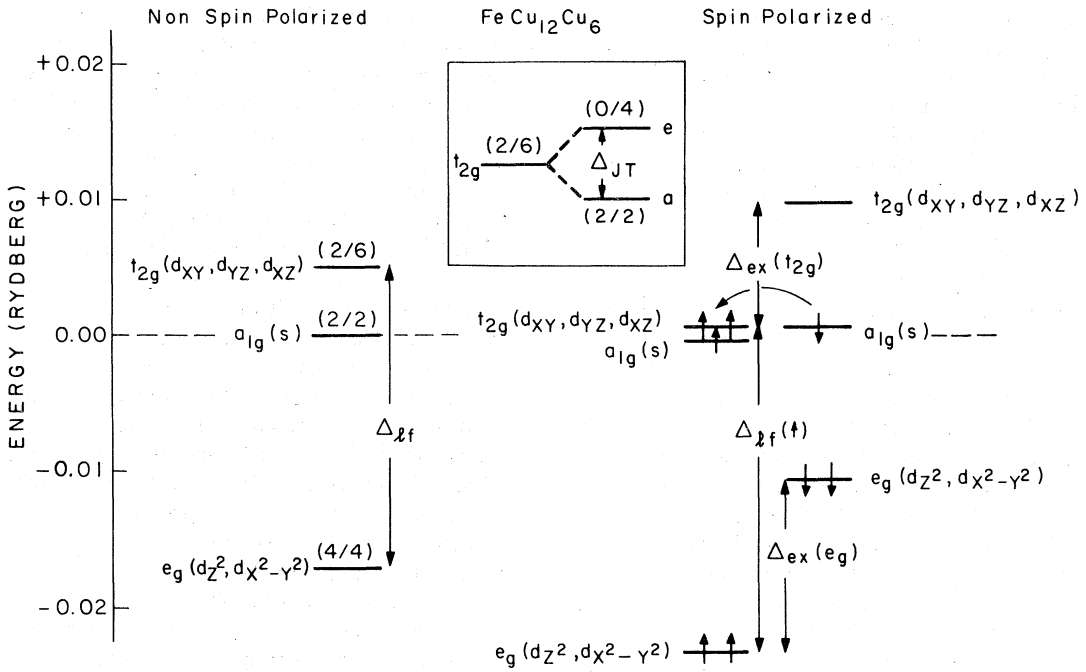

FIG. 12. Comparison of spin-polarized and non-spin-polarized energy levels for the highest three occupied molecular orbitals of the $FeCu_{12}Cu_6$ cluster (the $5e_g$, $5t_{2g}$, and $3a_{1g}$ levels in Fig. 5), displayed on a relative energy scale. The levels are labeled according to the principal partial-wave components on the Fe-impurity atom, and the level occupancies are indicated. The exchange splittings, $\Delta_{ex}(e_g)$ and $\Delta_{ex}(t_{2g})$, are an order of magnitude smaller than previous estimates based on the Anderson model and are also smaller than the ligand-field splitting Δ_{lf}. Possible excitations from the spin-down a_{1g} (s) orbital that is the discrete cluster analog of the half-filled conduction band of crystalline copper to the partially occupied degenerate spin-up $t_{2g}(d_{xy}, d_{yz}, d_{xz})$ orbital, corresponding to spin fluctuations on the impurity, are indicated by the arrow (see text). A possible Jahn-Teller splitting Δ_{JT} of the degenerate $t_{2g}(d_{xy}, d_{yz}, d_{xz})$ orbital is shown in the inset.

result is the small exchange splitting of those molecular orbitals, $e_g(d_{z^2}, d_{x^2-y^2})$ and $t_{2g}(d_{xy}, d_{yz}, d_{xz})$, containing the largest amount of Fe d-orbital character, namely, $\Delta_{ex}(e_g) = 0.17$ eV and $\Delta_{ex}(t_{2g}) = 0.12$ eV. These values are only a small fraction of the exchange splitting (~5 eV) for an isolated Fe atom and the exchange splitting assumed in the original Anderson model[5] and more recent models[1,2,12] for magnetic transition-metal impurities. The exchange splittings in Fig. 12 are also an order of magnitude smaller than the value (~2.5 eV) calculated by the SCF-$X\alpha$-SW method for the "d band" of a $FeFe_8Fe_6$ cluster representing ferromagnetic crystalline α-iron (see discussion in Sec. II). This unusual finding is a result of the overwhelming importance of the above-described covalent bonding-antibonding interaction of the Fe impurity d orbitals with the dsp hybrid orbitals on the surrounding Cu atoms, a factor that has been largely ignored in all previous theoretical models for magnetic impurities,[1-6] including Hirst's ion crystal-field model.[8] This result further suggests that various parameters in the often-used Anderson Hamiltonian for magnetic impurities, e.g., the Coulomb interaction parameter U usually identified with a large exchange splitting, should be redefined (see Sec. V).

Because the "spin-up" $a_{1g}(s)$ level in Fig. 12 corresponds to a cluster-renormalized Fe 4s-like orbital, whereas the "spin-down" $a_{1g}(s)$ level is the discrete cluster analog of the half-filled conduction band of crystalline copper (see Sec. III and Fig. 1), these levels describe an effective antiferromagnetic coupling between a "spin-up" electron on the Fe impurity site and a "spin-down" electron in the copper conduction band. The $t_{2g}(d_{xy}, d_{yz}, d_{xz})$ spin-up orbital is also effectively coupled antiferromagnetically to the copper conduction band as a result of self-consistency, although a nonmagnetic ground state at $T = 0\,^{\circ}K$ is not attained unless through Jahn-Teller effects of the type described in Ref. 47, or through a spin-

orbit coupling of the type described in Sec. VI. Thus the cluster spin orbitals exhibit some aspects of the antiferromagnetic coupling between the Fe impurity spin and "spin-compensation cloud" of the surrounding Cu atoms, often speculated to be responsible for the collapse of Curie Weiss magnetism below the Kondo temperature,[1,2] but the actual compensation is small relative to the net spin of the $t_{2g}(d_{xy}, d_{yz}, d_{xz})$ orbital in agreement with NMR studies of Boyce and Slichter.[12] The almost exact degeneracy of the partially occupied (2/3) spin-up $t_{2g}(d_{xy}, d_{yz}, d_{xz})$ orbital and fully occupied (1/1) spin-down $a_{1g}(s)$ orbital suggests that for $T \sim T_K$ there is a high probability of thermally induced excitations between the latter and former spin-orbitals, which in conventional solid-state many-body terminology correspond to "spin-flip" excitations between the copper conduction band at the Fermi energy and virtual Fe impurity d orbitals. These excitations imply fluctuations between cluster spin states of $S=1$ (two unpaired spins in t_{2g}) and $S=2$ (three unpaired spins in t_{2g} and one unpaired spin in a_{1g}) (see Fig. 12), yielding an average spin component of $S_z = 3/2$ on the $FeCu_{12}Cu_6$ cluster. Alternatively, promotion of an electron from the spin-up $a_{1g}(s)$ orbital to the nearly degenerate spin-up $t_{2g}(d_{xy}, d_{yz}, d_{xz})$ orbital, accompanied by spin fluctuations between the $a_{1g}(s)$ spin orbitals, also yields a spin component of $S_z = 3/2$ and a total of seven electrons in the $e_g(d_{x^2}, d_{x^2-y^2})$ and $t_{2g}(d_{xy}, d_{yz}, d_{xz})$ molecular orbitals (see Fig. 12). Magnetic susceptibility studies for Fe impurities in crystalline copper do indeed suggest a local magnetic moment corresponding approximately to a spin component of $S_z = 3/2$,[1] and our predicted integer value of seven electrons in the Fe impurity molecular orbitals is in agreement with the value deduced by Slichter and coworkers[12] from NMR studies.

Dickens *et al.*[11] have recently suggested, on the basis of neutron-diffraction studies of the CuFe Kondo system, that the spin-compensation-cloud model for the collapse of Curie-Weiss magnetism below the Kondo temperature could be made compatible with the alternative theory based on localized spin fluctuations (the LSF model) if the polarizable part of the compensation cloud, generally viewed as being of long-range character, were shrunk to the dimension of the 4s electron shell. The present $FeCu_{16}Cu_6$ cluster model is automatically compatible with both the spin-compensation-cloud and LSF models, since the spin-down $a_{1g}(s)$ orbital corresponding to the compensation cloud in the cluster is spatially indistinguishable from a renormalized Fe 4s orbital, whereas the above-described spin-flip excitations among the $a_{1g}(s)$ and spin-up $t_{2g}(d_{xy}, d_{yx}, d_{xz})$ orbitals around the Kondo temperature are equivalent to localized spin fluctuations. However, it should be emphasized that the present theoretical model does not yield a nonmagnetic ground state below the Kondo temperature unless the above-described Jahn-Teller effects and/or spin-orbit coupling described in Sec. VI are operative.

Thus the spin-polarized electronic structure of a $FeCu_{12}Cu_6$ cluster exhibits the principal measured characteristics of the local magnetic moments of Fe impurities in crystalline copper, while leading to radically new conclusions about the relative magnitudes of covalent and exchange interactions. Although the Kondo problem has been approached traditionally in terms of formal many-body theory,[1-3,9,10] it is not surprising that $FeCu_{12}Cu_6$ cluster spin-orbital eigenstates, determined from first principles by the SCF-$X\alpha$ method, should constitute a realistic basis for attacking this problem. First, the SCF-$X\alpha$ cluster molecular-orbital method goes beyond conventional Hartree-Fock theory in describing the local effects of both exchange *and* correlation,[14-17] and the electronic energy eigenvalues are rigorously defined as derivatives of the total energy with respect to occupation number,[14,15]

$$\epsilon_{ix\alpha} = \frac{\partial E}{\partial n_i} \tag{1}$$

in analogy to the definition of quasiparticle energies in Fermi-liquid theory.[48] Excitation energies, including the effects of spin-orbital relaxation and averaging over multiplets, follow from expression (1) in the SCF-$X\alpha$ method through the "transition-state" concept.[14,15] The claim that the SCF-$X\alpha$ technique goes beyond the Hartree-Fock method in accounting for correlation effects within the framework of a single-particle representation, including excited states, is supported by detailed quantitative comparison of results for polyatomic molecules with measured electronic and optical spectra and with the results of more elaborate theoretical approaches that systematically correct for correlation errors in Hartree-Fock theory via configuration-interaction or many-body perturbation theory.[17,49] Second, the cluster molecular-orbital method automatically includes the interaction of the transition-metal impurity d orbitals with localized d orbitals (as well as delocalized s- and p-like contributions) on the surrounding copper atoms, whereas such effects are completely neglected in the conventional "s-d" model[1-5] which views the transition-metal impurity d orbitals as interacting with purely s-like conduction electrons of the host metal.

Further support for the cluster molecular-orbital approach follows from the study of Mn impurities in copper. This system is of consider-

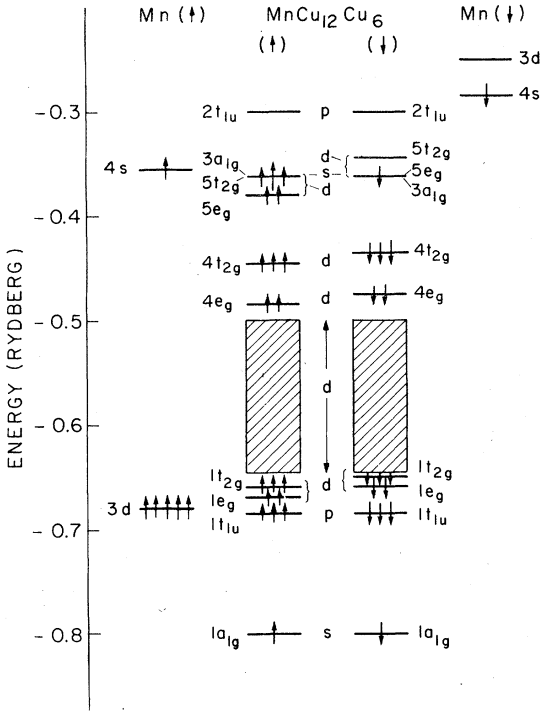

FIG. 13. Spin-polarized molecular-orbital energy levels of a $MnCu_{12}Cu_6$ cluster representing an isolated Mn impurity in crystalline copper. The most important bonding and antibonding spin orbitals are labeled in a fashion analogous to those shown for the $CuCu_{12}Cu_6$ cluster in Fig. 1, with the largely unperturbed copper d band indicated by the shaded regions. The spin-polarized Mn atomic orbitals are shown for comparison. Notable is the small exchange splitting of the $MnCu_{12}Cu_6$ cluster $5e_g(d)$ and $5t_{2g}(d)$ spin orbitals (the discrete analogs of the Friedel-Anderson virtual impurity states) in comparison with the exchange splitting of the Mn atomic $3d$ spin orbitals. The largest part of the electron-electron interaction in the cluster is associated with the large splitting between the bonding $(1e_g, 1t_{2g})$ and antibonding $(5e_g, 5t_{2g})$ orbitals. Note that the slightly longer arrow in the degenerate spin-up $5t_{2g}(d)$ and $3a_{1g}(s)$ orbitals represents *two* electrons.

able interest because, in addition to the existence of experimental data concerned with local magnetic moments and the Kondo effect,[1-3] there are optical absorption[50] and photoemission[51] spectra that have been used to determine the approximate positions of the Mn impurity states with respect to the Fermi level. Recently, Cohen and Slichter[12] have proposed a theoretical model, based on a three-parameter one-electron screened atomic potential with exchange, for explaining NMR satellite data for Mn, Fe, and other transition-metal impurities in copper.

An SCF-$X\alpha$-SW cluster molecular-orbital study of a representative $MnCu_{12}Cu_6$ cluster similar to the study of the $FeCu_{12}Cu_6$ cluster described above, leads to the spin-polarized electronic structure shown in Fig. 13. Only those energy levels for molecular orbitals with appreciable Mn components are fully labeled and their spin occupancy indicated. The largely unperturbed non-spin-polarized portions of the copper d-orbital manifold (the "d band") are indicated by the shaded regions. The $1e_g$ and $1t_{2g}$ spin orbitals near the bottom of the d band have significant bonding Mn d-orbital components; the contributions of Mn to the $4e_g$ and $4t_{2g}$ spin orbitals near the top of the d band are antibonding with respect to the nearest-neighbor Cu atoms and bonding with respect to second-nearest neighbors; the half-filled $5e_g$ and $5t_{2g}$ spin-orbitals are largely localized on the Mn impurity but have significant antibonding Cu components. Although contour maps of these orbitals are not included in this paper, they exhibit features analogous to those shown in Figs. 8–10 for the corresponding orbitals of $FeCu_{12}Cu_6$.

Also displayed in Fig. 13, for comparison, are the spin-orbital energy levels of a free Mn atom in a $(3d)^5(4s)^2$ configuration, as determined by the SCF-$X\alpha$ method, leading to a net atomic spin of $S = 5/2$. Like the results described above for the $FeCu_{12}Cu_6$ cluster (Fig. 12), the most immediately striking feature in Fig. 13 is the extremely small net exchange splitting of the $MnCu_{12}Cu_6$ cluster energy levels relative to the atomic exchange splitting. Nevertheless, if one applies Hund's rules to the cluster molecular orbitals, an effective "renormalized" $(3d)^5(4s)^2$ configuration and net magnetic moment of $5\mu_B$ for the $MnCu_{12}Cu_6$ cluster are attained as a consequence of five unpaired electrons in the spin-up $5e_g(d_{z^2}, d_{x^2-y^2})$ and $5t_{2g}(d_{xy}, d_{yz}, d_{xz})$ molecular orbitals and spin-paired $3a_{1g}(s)$ orbitals. Note also in Fig. 13 that promotion of an electron from the spin-down $3a_{1g}(s)$ orbital to the nearly degenerate spin-down $5e_g(d_{z^2}, d_{x^2-y^2})$ orbital does not change the net spin of the cluster. Since the spin-down $3a_{1g}(s)$ orbital can be interpreted as the discrete cluster analog of the half-filled conduction-band of crystalline copper around the Fermi level, as described in Sec. III (see Fig. 1), the cluster electronic structure in Fig. 13 mimics the weak antiferromagnetic coupling of the Mn impurity with the copper conduction band in much the same fashion as described above for the CuFe system (Fig. 12). Thus the $MnCu_{12}Cu_6$ cluster electronic structure is consistent with magnetic susceptibility data for Mn impurities in copper[1] which show an effective local magnetic moment of $5\mu_B$, close to the free-atom value. In other words, the large exchange splitting associated with the $(3d)^5(4s)^2$ configuration of the free Mn atom, often assumed by other workers[1,2,12] on the basis of the Ander-

son model[5] to be of the same order of magnitude for Mn impurities in crystalline copper, is actually compensated for and replaced by the significant bonding-antibonding interaction of the impurity with its local crystalline environment, which then leads, in conjunction with Hund's rules, to an effective $(3d)^5(4s)^2$-like $MnCu_{12}Cu_6$ cluster molecular-orbital configuration and magnetic moment of $5\mu_B$. It should be emphasized again that such effects are quite common in transition-metal coordination chemistry,[28,29] and it is therefore not surprising that they should be important in transition-metal alloys. Except for the ion crystal-field model of Hirst,[8] which, however, neglects molecular-orbital formation, and simple models for charge transfer between alloy constituents,[37] the possible role of transition-metal coordination chemistry in determining local magnetic moments and other electronic properties of dilute alloys has not been considered in previous theoretical models.[1-10]

The electronic structure of the $MnCu_{12}Cu_6$ cluster shown in Fig. 13 thus suggests alternative explanations of spectroscopic, magnetic, and transport data for dilute CuMn alloys. For example, the photoelectron spectrum of such alloys (for photon energy 10.2 eV)[51] is similar to that for pure copper, except for some enhancement of photoemission intensity near the bottom of the d band and small changes in spectral character between the top of the d band and Fermi level. The conventional explanation of these data is that the filled spin-up Mn-3d impurity states lie well below the Fermi level and that there is a large exchange splitting between the filled spin-up and empty spin-down impurity states.[51] In contrast, the $MnCu_{12}Cu_6$ cluster electronic structure shown in Fig. 13 suggests that the differences between the photoemission spectra of dilute CuMn alloys and pure copper are due to the presence of Mn d-orbitals bonding character (the $1e_g$ and $1t_{2g}$ levels) near the bottom of the d band and Mn d-orbital antibonding character (the $4e_g$ and $4t_{2g}$ levels) near the top of the d band. The predicted Mn d-orbital character in the spin-up $5e_g$ and $5t_{2g}$ orbitals near the cluster Fermi level is not evident in the published (10.2 eV) photoemission spectrum,[51] although an enhancement of photoemission intensity associated with such orbitals should be observed for higher photon energies.

The optical absorption spectrum of dilute CuMn alloys is also very similar to that of pure copper, showing an onset of absorption around 2 eV and a second absorption peak around 5 eV.[50] This spectrum has been argued to be consistent with either a very small exchange splitting of Mn 3d impurity states around the Fermi level[50] or a large (~5 eV) exchange splitting of these states.[51] The $MnCu_{12}Cu_6$ cluster electronic structure shown in Fig. 13, in conjunction with the SCF-$X\alpha$ transition-state concept,[14,15] suggests that the onset of optical absorption at 2 eV is associated with allowed electronic transitions from the occupied antibonding d orbitals ($4e_g$, $4t_{2g}$) near the top of the d band to empty antibonding p orbitals ($2t_{1u}$) just above the Fermi level, which correspond to optical transitions between the top of the d band and Fermi level in pure crystalline copper. The 5-eV absorption peak is assigned to transitions from the occupied bonding d orbitals ($1e_g$, $1t_{2g}$) near the bottom of the d band to the unoccupied antibonding p orbitals ($2t_{1u}$) immediately above the Fermi level. These transitions are summarized in Table III. Allowed transitions from the main part of the copper d band (the shaded regions in Fig. 13) to empty states above the Fermi level should account for optical absorption between 3 eV and 5 eV.

TABLE III. Allowed optical transitions (in the visible and near-ultraviolet regions of the spectrum) between spin orbitals of the $MnCu_{12}Cu_6$ cluster, as determined by the transition-state procedure.

Orbital transition	Transition energy (eV)
$4t_{2g}(d)\downarrow \rightarrow 2t_{1u}(p)\downarrow$	2.1
$4t_{2g}(d)\uparrow \rightarrow 2t_{1u}(p)\uparrow$	2.3
$4e_g(d)\downarrow \rightarrow 2t_{1u}(p)\downarrow$	2.7
$4e_g(d)\uparrow \rightarrow 2t_{1u}(p)\uparrow$	2.8
$1t_{2g}(d)\downarrow \rightarrow 2t_{1u}(p)\downarrow$	5.1
$1e_g(d)\downarrow \rightarrow 2t_{1u}(p)\downarrow$	5.2
$1t_{2g}(d)\uparrow \rightarrow 2t_{1u}(p)\uparrow$	5.2
$1e_g(d)\uparrow \rightarrow 2t_{1u}(p)\uparrow$	5.3

The degeneracy of the spin-up $5t_{2g}(d)$ and spin-down $5e_g(d)$ impurity orbitals with the $3a_{1g}(s)$ orbitals that are cluster analogs of conduction-band states at the Fermi level suggest the possibility of spin fluctuations at very low temperatures of the order of the Kondo temperature for Mn impurities in copper. Such fluctuations have been connected with the increase of electrical resistivity with decreasing temperature around the low-temperature resistance minimum associated with the Kondo effect.[1-3,9,10] The cluster electronic structure shown in Fig. 13 is consistent with the observed low-temperature resistance minimum to the extent that it is also consistent with an antiferromagnetic exchange Hamiltonian of the type $J\vec{S}\cdot\vec{s}$ (negative J), as used by others to explain the resistance minimum.[1-3,9,10] The possible use of the cluster spin orbitals as a basis for parametrizing a $J\vec{S}\cdot\vec{s}$ Hamiltonian is discussed in Sec. V B of

this paper. The residual resistivity of dilute CuMn alloys, along with the resistivities of dilute CuFe and CuV alloys, is more directly explained in terms of the electron scattering properties (e.g., partial-wave phase shifts) of the $MnCu_{12}Cu_6$, $FeCu_{12}Cu_6$, and $VCu_{12}Cu_6$ clusters, as described in Sec. IV D.

Although we have not yet fully investigated the use of the $MnCu_{12}Cu_6$ and $FeCu_{12}Cu_6$ electronic structures as a basis for explaining the NMR data of Slichter and co-workers[12] for Mn and Fe impurities in copper, preliminary calculations suggest that good agreement with their measured Knight shifts can be obtained if the parameters in their theory (the widths and positions of the spin-up and spin-down impurity levels) are reformulated in terms of the cluster molecular spin orbitals. Since the Knight-shift formula and parameters provided by Slichter and co-workers,[12] are based on the Friedel-Anderson model,[4,5] a redefinition of these parameters on the basis of the cluster electronic structures is equivalent to the reformulation of the Anderson Hamiltonian[5] itself to take account of the effects of the covalency and much reduced exchange splitting implied in Figs. 12 and 13. Such a reformulation of the Anderson Hamiltonian is proposed in Sec. V A. Except for the 43-atom copper cluster considered in Sec. VII in connection with the renormalization-group approach, the clusters ($MnCu_{12}Cu_6$ and $FeCu_{12}Cu_6$) used in these studies simulate the environments of the impurity only out to second-nearest neighbors. Nevertheless, the Knight shift formula,[12] once parametrized on the basis of the cluster electronic structures, can then be used to interpret the NMR satellite data out to many more shells of atoms surrounding the impurity, in much the same fashion as recently demonstrated by Cohen and Slichter[12] using a three-parameter modified impurity atomic potential.

D. Residual electrical resistivity

Apart from the low-temperature contribution of the Kondo effect to the electrical resistance,[1-3,9] the ordinary "residual" resistivity of a metal such as copper containing transition-metal impurities has been traditionally interpreted within the framework of Friedel's[4] concept of virtual impurity states, through the partial-wave scattering of the host-metal conduction electrons by the isolated impurity atoms, leading to an expression for the impurity resistivity of the form[3]

$$R_{\rm imp} = R_0 c \sum_l (2l+1) \sin^2[\eta_l(\epsilon_F) - \eta_{l-1}(\epsilon_F)], \quad (2)$$

where

$$R_0 = 4\pi h/e^2 k_F \quad (3)$$

is the "unitarity limit" resistivity, c is the impurity concentration, and $\eta_l(\epsilon_F)$ is the scattering phase shift for the lth partial wave of energy in the vicinity of the Fermi energy ϵ_F.

For magnetic impurities, the above expression can be generalized to account for the scattering from the two independent channels corresponding to the spin-split virtual impurity states and can be simplified by neglecting the nonresonant phase shifts corresponding to $l=0$ (s) and $l=1$ (p) partial waves, resulting in the formula[3]

$$R_{\rm imp} = R_0 c \tfrac{5}{2}[\sin^2\eta_{2\uparrow}(\epsilon_F) + \sin^2\eta_{2\downarrow}(\epsilon_F)]. \quad (4)$$

The "spin-up" and "spin-down" $l=2$ "resonant" phase shifts, $\eta_{2\uparrow}(\epsilon_F)$ and $\eta_{2\downarrow}(\epsilon_F)$, respectively, are related by the Friedel sum rule[4] to the occupation numbers, $n_{d\uparrow}$ and $n_{d\downarrow}$, respectively, of the d-like virtual impurity spin orbitals, giving

$$\eta_{2\uparrow}(\epsilon_F) = n_{d\uparrow}\pi/5\,, \quad (5)$$

$$\eta_{2\downarrow}(\epsilon_F) = n_{d\downarrow}\pi/5\,. \quad (6)$$

Expressions (4)–(6) qualitatively account for the familiar double-peaked curve describing the room-temperature residual resistivity of transition-metal impurities in a copper host, as one progresses through the transition series from Ti to Ni, with a resistivity minimum for Mn impurities (where $n_{d\uparrow}=5$ and $n_{d\downarrow}=0$), maxima near V and Fe, and nearly zero resistivity for Ni impurities (see Fig. 5 of Ref. 3).

As shown in preceding sections of this paper, the $5e_g(d_{z^2}, d_{x^2-y^2})$ and $5t_{2g}(d_{xy}, d_{yz}, d_{xz})$ molecular orbitals of a coordinatively saturated cluster of the type $MCu_{12}Cu_6$ representing the local environment, up to second-nearest neighbors, of a transition-metal impurity (M = Ni, Fe, V, Mn) in crystalline copper (see Figs. 5 and 13) are discrete analogies of the Friedel-Anderson[4,5] virtual impurity states, satisfy a sum rule analogous to the Friedel sum rule,[4] and for magnetic impurities such as Fe and Mn are spin split more or less symmetrically around the cluster Fermi energy (see Figs. 12 and 13), albeit by an amount an order of magnitude smaller than previous estimates[1,2,5,12] due to covalent bonding effects. We can straightforwardly extend Friedel's[4] concept of partial-wave scattering from the isolated impurity atom (M) to the impurity-host cluster ($MCu_{12}Cu_6$), generalizing the resonant scattering phase shifts of expression (4) to the cluster $5e_g(d_{z^2}, d_{x^2-y^2})$ and $5t_{2g}(d_{xy}, d_{yz}, d_{xz})$ spin orbitals. Indeed, the multiple-scattered-wave formalism[16] underlying the SCF-$X\alpha$-SW cluster molecular-orbital method[14] describes the eigenstates of a cluster or molecule as the "resonant bound states"

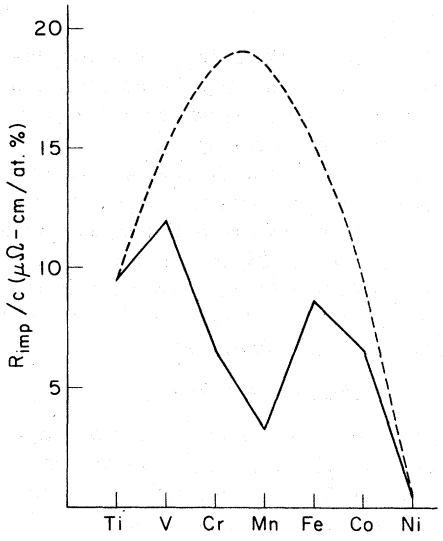

FIG. 14. Residual electrical resistivities associated with transition-metal impurities in copper, calculated on the basis of impurity cluster molecular-orbital partial-wave scattering phase shifts. The solid lines correspond to room-temperature (300 °K) magnetic-impurity configurations, whereas the dashed curve corresponds to the low-temperature (0 °K) nonmagnetic configurations.

of a scattering matrix.

Applying Eq. (4) to the appropriate spin-polarized cluster $5e_g$ and $5t_{2g}$ orbital configurations (of the type shown in Fig. 13) for the Fe, Mn, and V impurities in their "magnetic states," and to interpolated configurations for magnetic Cr and Co impurities (for which detailed cluster models have not been calculated), we obtain the resistivity profile shown by the solid lines in Fig. 14. On an absolute scale, this profile is in good agreement with room-temperature (300 °K) data for dilute Cu-based alloys shown in Figs. 5 and 22 of Ref. 3. For those impurities, e.g., Ni and Ti, which do not exhibit magnetic moments in copper and for the other impurities at $T = 0$ °K, where the magnetic moments are quenched because of the Kondo effect, it is more appropriate to use the non-spin-polarized Eq. (2) and non-spin-polarized cluster orbital configurations of the type shown in Fig. 5. This yields the dashed resistivity curve displayed in Fig. 14, which is in reasonable agreement with low-temperature resistivity data shown in Fig. 22 of Ref. 3.

An alternative procedure would be to calculate the electron-cluster scattering cross sections using the SCF-$X\alpha$-SW computational technique recently developed by Davenport *et al.*[52] for determining electron-molecule scattering cross sections.

V. MODEL HAMILTONIANS

A. Reformulation of the Anderson Hamiltonian

One of the most widely used theoretical models for magnetic impurities in metallic hosts is the Anderson Hamiltonian,[5] which has the well-known form

$$H_A = \sum_{km} \epsilon_k n_{km} + \sum_m \epsilon_d n_{dm} + \sum_{km} V_{kd}(c_{km}^* c_{dm} + c_{dm}^* c_{km}) + U n_{d\uparrow} n_{d\downarrow}, \quad (7)$$

where

$$n_{km} = c_{km}^* c_{km}, \quad n_{dm} = c_{dm}^* c_{dm}. \quad (8)$$

The first two terms of this Hamiltonian are the contributions of the conduction electrons and impurity d electrons, respectively, whereas V_{kd} represents the mixing interaction between the conduction electrons and d electrons (the so-called s-d interaction). The last term in (7) represents the Coulomb repulsion between impurity d electrons of opposite spin, where U has been identified traditionally with a large (several eV) exchange splitting of the impurity spin orbitals.[5,1-3,12] The condition for the existence of a local magnetic moment in the Anderson model[5] is that U be significantly larger than the "width" Δ associated with the virtual impurity d orbital, i.e.,

$$U/\Delta \gg 1. \quad (9)$$

The width parameter Δ cannot be determined directly from experiment, although estimates based on combined experimental-theoretical inference give an upper limit of $\Delta \sim 0.5$–0.6 eV for Fe-group impurities in copper.[1]

As described in Sec. IV C (Figs. 12 and 13), one of the most striking features of the present cluster models for local magnetic moments is that the exchange splitting of the spin orbitals associated with the transition-metal impurity is an order of magnitude smaller than previous estimates,[5,6,1-3,12] as a consequence of the dominant role of the coordination-chemical bonding-antibonding interaction of the impurity with its local crystalline environment. The latter interaction, represented approximately in Fig. 13 for Mn in copper by the average difference in energy of ~0.3 Ry (~4 eV) between the $(1e_g, 1t_{2g})$ bonding orbitals and $(5e_g, 5t_{2g})$ antibonding impurity orbitals, contributes the largest part of the Coulomb energy U, leaving only a relatively small contribution (~0.6 eV) due to the exchange splitting of the spin-up and spin-down $(5e_g, 5t_{2g})$ impurity levels more or less symmetrically around the Fermi level. Thus the total Coulomb repulsion, arising from the contributions

of antibonding interaction and exchange splitting, is of the same order of magnitude (~5 eV) as that based exclusively on exchange splitting in the original Anderson model[5] and subsequent applications thereof.[1-3,12] The bonding-antibonding contribution to U can be incorporated into the second term of the Anderson Hamiltonian (7) as an effective potential V^i that splits the degenerate impurity atomic d-orbital energy level ϵ_d into bonding ($i=b$) and antibonding ($i=a$) levels, suggesting the new model Hamiltonian

$$H_{\text{new}} = \sum_{km} \epsilon_k n_{km} + \sum_{mi} (\epsilon_d + V^i) n_{dm} + \sum_{km} V^a_{km}(c^*_{km}c_{dm} + c^*_{dm}c_{km}) + \tilde{U} n_{d\uparrow} n_{d\downarrow} , \quad (10)$$

where $\tilde{U}$ now represents the much reduced exchange splitting of the impurity spin orbitals around the Fermi energy. The quantity V^a_{km} describes the mixing of the impurity d orbitals with the s,d-hybrid orbitals on the surrounding metal atoms, as determined by the partial-wave decomposition of the cluster molecular orbitals (see Table II), and replaces the s-d mixing interaction in the original Anderson Hamiltonian (7). The conceptual advantage of this new model Hamiltonian is that the largest component of the Coulomb interaction is absorbed into a one-electron term, leaving only a relatively small spin-splitting term $\tilde{U} n_{d\uparrow} n_{d\downarrow}$ that describes the formation of the local magnetic moment.

The present theoretical model is consistent with condition (9) for the onset of local magnetization if the original Friedel-Anderson[4,5] virtual impurity state width parameter Δ, corresponding to $U \sim 5$ eV, can be identified with the ligand-field splitting $\Delta_{\text{lf}} \sim 0.3$ eV of the $t_{2g}(d_{xy}, d_{yz}, d_{xz})$ and $e_g(d_{z^2}, d_{x^2-y^2})$ impurity orbitals around the Fermi level (see Fig. 12). The reduced spin-splitting interaction term $\tilde{U} \sim 0.2$–0.6 eV (Figs. 12 and 13) implies a proportionally smaller value of $\tilde{\Delta} \sim 0.01$–0.04 eV for the width of the individual $t_{2g}(d_{xy}, d_{yz}, d_{xz})$ level that is the cluster analog of the virtual impurity state. The small value of $\tilde{\Delta}$ is in accord with the spatial localization of the impurity molecular orbitals in the cluster and is of the same order of magnitude as the difference in energy between the discrete $t_{2g}(d_{xy}, d_{yz}, d_{xz})$ impuritiy orbital and the $a_{1g}(s)$ orbital that is the discrete cluster analog of the conduction band around the Fermi level. Thus the ratio $\tilde{U}/\tilde{\Delta}$ is of the same order of magnitude as U/Δ for Fe and Mn impurities in copper, and satisfies a relation

$$\tilde{U}/\tilde{\Delta} \gg 1 , \quad (11)$$

analogous to (9) for the occurrence of local magnetization.

Preliminary calculations suggest that the reformulated Anderson Hamiltonian (10), together with the parameters V^i, V^a_{km}, $\tilde{U}$, and $\tilde{\Delta}$ determined from the cluster electronic structures, can be used in much the same way as the original Anderson Hamiltonian (7) to interpret various physical properties associated with local magnetic impurities. For example, Slichter and coworkers[12] have recently interpreted NMR measurements for Mn and Fe impurities in copper using a formula for the Knight shift based on the Anderson-Friedel model, the parameters U and Δ, and a crystal-field parameter. Implicit in their theoretical analysis, including the most recent three-parameter atomic potential model of Cohen and Slichter,[12] is the identification of the large value of U(~5.6 eV) with the exchange splitting of the impurity d spin-orbitals. Since the $FeCu_{12}Cu_6$ and $MnCu_{12}Cu_6$ cluster electronic structures described above are clearly inconsistent with such identification, it is important for one to reinterpret the NMR data in terms of the present theoretical model. Preliminary results indicate that the Knight-shift expression of Slichter and co-workers[12] can indeed by reformulated in terms of the parameters of the model Hamiltonian (10), and such calculations are in progress as part of our continuing research.

B. The $J\vec{S}\cdot\vec{s}$ exchange Hamiltonian

As discussed in Sec. IV C, the spin-polarized electronic structures of the $FeCu_{12}Cu_6$ and $MnCu_{12}Cu_6$ clusters show an effective antiferromagnetic coupling of impurity d spin-orbitals with sd-hybrid spin orbitals on the surrounding Cu atoms that is analogous to, but considerably weaker and more spatially localized than, the antiferromagnetic coupling of the local magnetic moment with the "spin-compensation cloud" of the copper conduction band frequently speculated by others to be responsible for the Kondo effect.[1,2] An exchange Hamiltonian of the form[1,2,9]

$$H_K = -J\vec{S}\cdot\vec{s} , \quad (12)$$

where J is the negative Heisenberg exchange integral, $\vec{S}$ is the impurity spin, and $\vec{s}$ is the conduction-electron spin of the host metal, is often used to model the antiferromagnetic coupling of the transition-metal impurity to the conduction electrons. Slater[53] has shown that an SCF-$X\alpha$-SW cluster molecular-orbital representation of the electronic structure of an antiferromagnetic crystal can be used in conjunction with the "transition-state" concept as a basis for calculating, from first principles, the exchange integral in a Hamiltonian of the form (12) and for estimating the Neél temperature. In view of the formal similarity of

these two problems, it is possible that the $FeCu_{12}Cu_6$ and $MnCu_{12}Cu_6$ cluster electronic structures can be used to parametrize a Kondo Hamiltonian of the form (12), which can then be applied, in conjunction with perturbation theory,[9] to calculate the contribution of the Kondo effect to electrical resistivity and other transport properties at low temperatures. Indeed, the well-known expression for the Kondo temperature,[1-3]

$$T_K = T_F \exp[-1/|J|N(\epsilon_F)], \tag{13}$$

corresponding to the temperature at which perturbation theory for electrical resistivity based on the Hamiltonian (12) diverges, is the type of relation that might emerge from a connection between the cluster transition-state representation of J and thermally induced spin fluctuations between nearly degenerate spin orbitals around the Fermi level of the type described in Sec. IV C. This is largely speculation at this point and will be further investigated in our continuing studies. As shown in Sec. VI, spin-orbit coupling may also play a key role in determining low-temperature properties of magnetic impurities in metallic hosts.

VI. SPIN-ORBIT COUPLING AND THE QUENCHING OF THE LOCAL MAGNETIC MOMENT

In Sec. IV, it was shown that orbitals with considerable d amplitude on the impurity atom, which are antibonding with respect to the host cluster, occur at the Fermi level for magnetic impurities. An interesting question is the degree to which spin-orbit coupling will split such levels about the Fermi level and what the consequence of such an effect will be on temperature-dependent properties. This is in general a very complicated problem and one which we are not prepared to address in a completely adequate manner at the present time. Nonetheless, some insight can be gained by considering a very simple model. The model, which perhaps may be inappropriate to a detailed discussion of any specific experimental system, does suggest, however, that these effects which are normally ignored in the magnetic impurity problem should be investigated more thoroughly.

The simple model considered is the following: (i) assume that the ligand-field splitting Δ_{lf} of the $e_g(d_{z^2}, d_{x^2-y^2})$ and $t_{2g}(d_{xy}, d_{yz}, d_{xz})$ impurity levels near the Fermi energy (e.g., those shown in Fig. 12) is very much greater than the spin-orbit splitting; (ii) assume that the e_g manifold is occupied and only the t_{2g} manifold need be considered; (iii) assume initially the simple case of a $(t_{2g})^1$ configuration. With these assumptions, and for the moment ignoring the reduction of the orbital momentum, the magnetic susceptibility due to isolated impurity sites can be computed from the expression

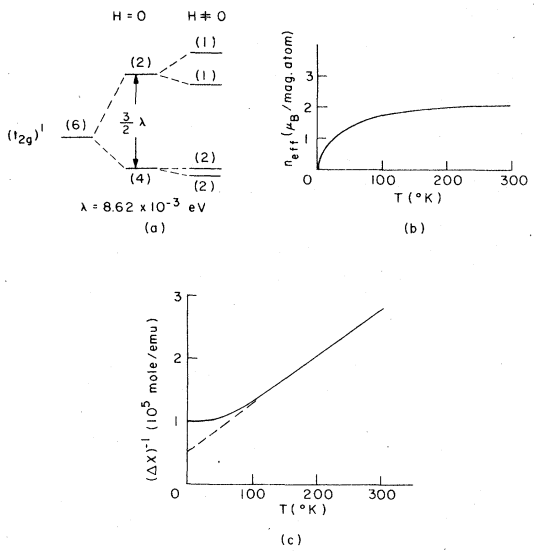

FIG. 15. (a) Spin-orbit splitting of a $(t_{2g})^1$ impurity cluster molecular-orbital configuration with and without an applied magnetic field H. The orbital degeneracies and spin-orbit energy λ are indicated. (b) Effective number of Bohr magnetons per magnetic impurity site as a function of temperature for the spin-orbit coupling implied in (a), showing the quenching of the impurity magnetic moment at low temperature. (c) Inverse magnetic susceptibility as a function of temperature for the spin-orbit coupling implied in (a), showing the collapse of Curie-Weiss behavior at low temperature.

$$\chi(T) = \frac{N\mu_B^2}{3kT}\left(\frac{8 + (3\lambda/kT - 8)e^{-3\lambda/2kT}}{\lambda/kT(2 + e^{-3\lambda/2kT})}\right). \tag{14}$$

This expression was first derived by Kotani[53] from the classic work of Van Vleck.[54] N is the number of magnetic sites, μ_B denotes the Bohr magneton, and λ is the spin-orbit energy. The energy level scheme arising from the $(t_{2g})^1$ configuration and which is used to derive the above magnetic susceptibility expression is shown in Fig. 15(a). The expression in the brackets of Eq. (14) is equal to the square of the effective number of Bohr magnetons, $n_{\text{eff}}^2(T)$, per magnetic site. Experimental susceptibility data for magnetic impurity systems are often plotted as $1/\chi(T)$ vs T to show the Curie-Weiss behavior above the so-called Kondo temperature.[1-3] In Figs. 15(b) and (c), the functions $n_{\text{eff}}(T)$ and $1/\chi(T)$, respectively, are shown, which have been deduced directly from Eq. (14). The value of λ used is 8.62×10^{-3} eV, which is about one half of the value appropriate for the isolated vandium atom.[55] The example of

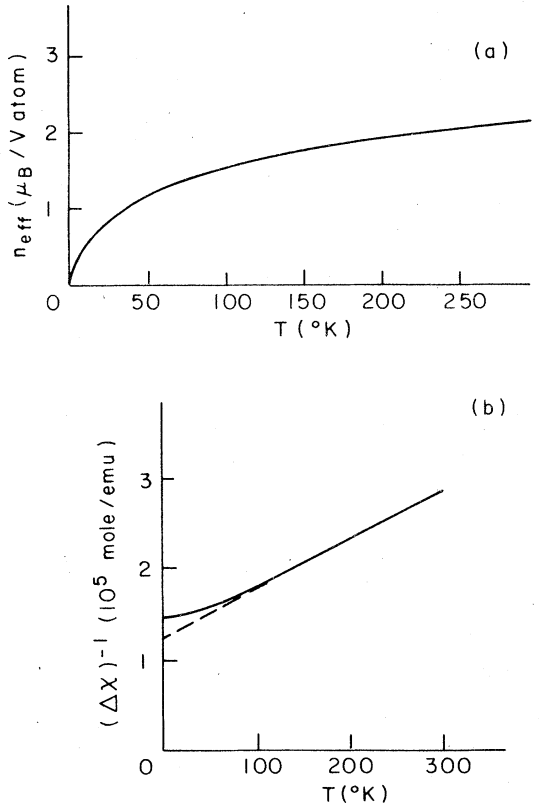

FIG. 16. Experimental results (see Refs. 56 and 57) for (a) the effective number of Bohr magnetons per magnetic impurity site and (b) the inverse magnetic susceptibility as functions of temperature for V impurities in a gold host, showing the quenching of the impurity magnetic moment and disappearance of Curie-Weiss behavior at low temperature.

V (rather than Fe or Mn) is chosen to generate the theoretical curves in Fig. 15 because the Kondo system of V impurities in a gold host has been thoroughly investigated experimentally,[56] leading to the curves for $n_{\rm eff}(T)$ and $1/\chi(T)$ in Fig. 16; this system has a relatively high Kondo temperature (~300°K) which allows for a wide temperature range over which the transition from Curie-Weiss magnetism to the nonmagnetic limit can be studied; and a $(t_{2g})^1$ electron configuration is a possible one for V impurities in gold. The V atomic λ value[55] is reduced by one half in Eq. (14) to account for the effects of electron delocalization in the t_{2g} molecular orbital, as is evident in the t_{2g} orbital contour map of Fig. 11. See also Table I.

The striking feature of Fig. 15(b) is that at low temperatures the magnetic moment is quenched in spite of the fact that the system has an unpaired spin. This, of course, arises from the effect of spin-orbit coupling on the ground state, which results in the cancellation of the spin and orbital momenta contributions to the magnetic moment. The quenching of the impurity magnetic moment at low temperatures (below the Kondo temperature) is one of the aspects of the Kondo effect.[1-3] In the past, it has always been attributed to local spin fluctuations at the impurity site or to an antiferromagnetically coupled spin-compensation cloud induced in the surrounding conduction electrons of the host metal. As we have shown in Sec. IV C, there is indeed some evidence for both these effects in the impurity cluster electronic structures, although they are not sufficient in magnitude to account for the complete cancellation of the impurity magnetic moment. However, the present spin-orbit coupling contribution to the electronic structure provides a possible alternative explanation for the quenching of the magnetic moment at low temperatures, at least in the simplest example. In general, however, the situation may be more complicated, and spin-orbit coupling might be only a contributing factor to the complete description of the temperature dependence of the magnetic moment.

In Fig. 15(c), the simple spin-orbit effect is shown to yield the characteristic Curie-Weiss behavior of the magnetic susceptibility at higher temperatures together with the anomalous low-temperature behavior usually associated with the "Kondo effect." The assumed concentration of impurity sites is 0.2 at.%. For comparison, we display in Fig. 16 the results of experiment for V impurities in a gold host, as measured by Van Dam *et al.*[56] for 0.2-at.% impurity concentration. The solid curve in Fig. 16(b) is a theoretical fit by Schotte and Schotte[57] to the experimental data of Van Dam *et al.*[56]; the dashed line is a linear extrapolation from the higher-temperature data showing the Curie-Weiss behavior in this regime. The theoretical treatment of Schotte and Schotte,[57] based on the "*s-d* exchange model," was characterized by Van Dam *et al.*[56] as "the first example where a theory can successfully describe the behavior of χ from $T=0$ up to $T=T_K$."

A comparison of Figs. 15 and 16 shows that the present spin-orbit coupling model, in conjunction with the impurity cluster electron structure, also seems to describe the observed magnetic properties of V impurities in a gold host. This it would appear that a more thorough investigation of the effects of spin-orbit coupling in such systems should be pursued. It may turn out that many aspects of the Kondo problem can be deduced from considerations of classical ligand-field theory.

It is instructive to explore some further consequences of the model introduced here, e.g., the relationship between the spin-orbit energy parameter λ and the temperature at which $1/\chi(T)$ deviates from Curie-Weiss behavior. It is straightforward to deduce from Eq. (14) that as λ decreases in magnitude, the temperature at which $1/\chi(T)$ deviates from Curie-Weiss dependence decreases, i.e., the "Kondo" temperature decreases. Upon going from Ti to Ni across the first transition series of the Periodic Table, the magnitude of λ increases.[55] However, there is another effect evident from the cluster molecular-orbital models of Sec. IV; namely, the amplitude of the $t_{2g}(d_{xy}, d_{yz}, d_{xz})$ orbital near the Fermi energy found on the impurity atom decreases across this series (see entries for $5t_{2g}$ orbital in Table I). Such a decrease in amplitude on the impurity site sould reduce λ from its free-atom value; hence the value of λ that is appropriate in the metallic host environment will be determined by a balance between these two factors. Another effect to consider is the partial quenching of orbital angular momentum on the impurity atom. This effect should be larger for cases where the d amplitude of the t_{2g} level on the impurity atom is small. This can be taken into account by employing "orbital reduction factors" in the derivation of the magnetic susceptibility expression. One then arrives at a modified form of Eq. (14) which leads to changes in the calculated quantities in Figs. 15(b) and (c), as briefly discussed below.

The main effect of the orbital reduction factor is to keep the spin and orbital contributions to the magnetic moment from completely cancelling in the ground state. This means that Fig. 15(b) will be modified (although the general shape remains the same) such that n_{eff} no longer goes to zero at $T = 0\,^{\circ}\text{K}$ but retains a finite value that depends on the reduction factor. The high-temperature limit of n_{eff} is likewise reduced with the reduction factor. This effect on $1/\chi(T)$ shown in Fig. 15(c) is to increase the slope of the Curie-Weiss portion of the curve (due to the reduction of n_{eff} at high temperatures) and to modify the low-temperature properties. In particular, the value of $1/\chi(T)$ at $T = 0\,^{\circ}\text{K}$ is no longer a finite value, but zero. The resulting curve looks very similar to Fig. 15(c), except at very low temperatures, where the curve turns over and goes to zero at $T = 0\,^{\circ}\text{K}$.

One may wonder if the $(t_{2g})^1$ configuration is not a very special case and therefore irrelevant to the general problem. The fact is, however, that its behavior is characteristic of other $(t_{2g})^n$ configurations as shown in Fig. 17. In Fig. 17, the quantity $n_{\text{eff}}(T)$ is plotted for the various $(t_{2g})^n$ configurations which possess a magnetic moment. It is seen that with the exception of $(t_{2g})^3$, these configurations also exhibit a decrease in the magnetic moment, i.e., a partial quenching, at low temperatures. Furthermore, since the magnetic susceptibility is given by

$$\chi(T) = N n_{\text{eff}}^2 / 3kT \tag{15}$$

it is clear that, while the $(t_{2g})^3$ configuration gives a Curie behavior over the complete temperature range, the other configurations will yield a Curie-like dependence at high temperatures with anomalous behavior at low temperatures similar to that discussed above for the $(t_{2g})^1$ configuration.

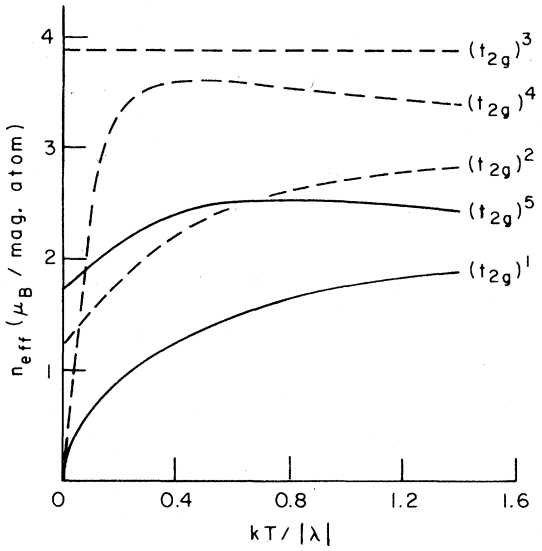

FIG. 17. Temperature dependence of the effective number of Bohr magnetons per magnetic impurity site for various configurations of the impurity cluster $t_{2g}(d_{xy}, d_{yz}, d_{xz})$ molecular orbital.

The type of behavior shown in Fig. 17 is not limited to the strong or intermediate ligand-field limit but is also found[58] in the weak-field limit where $(t_{2g})^m(e_g)^n$ configurations have to be considered, as well as in cases where static and dynamic Jahn-Teller effects are present.[47] Thus the partial quenching of the magnetic moment at low temperatures is a phenomenon found in a wide variety of configurations, and hence the discussion given above for the $(t_{2g})^1$ case is more or less representative of a general situation. With this in mind, one might choose such a configuration, consider it as a phenomenological model, and pursue its consequences. This is presently being done for a number of other anomalous properties, including transport properties and specific heat,

associated with the Kondo effect,[1-3,9] and will be reported in detail in a future paper. Suffice it to say here that an impurity orbital energy level structure near the Fermi energy such as that illustrated in Fig. 15(a) can be shown to give rise in a very simple way to a number of the anomalous temperature-dependent properties associated with the Kondo effect.

VII. CLUSTER RENORMALIZATION AND THE RENORMALIZATION-GROUP METHOD

One of the most recent developments in solid-state theory has been the application of the renormalization-group method[13] to the Kondo problem. The essence of this approach is the use of a renormalization-group transformation to set up a sequence of model Hamiltonians containing terms of the form (12) to describe the coupling of the magnetic impurity to the crystal conduction band on multiple energy scales around the Fermi level. This procedure is implemented computationally through the use of a Wannier-type basis localized on successive spherical shells centered on the impurity site.[13]

With regard to the general notion that surrounding shells of atoms have a "renormalizing" effect on the impurity-atom electronic structure and spin polarization, the cluster approach described in this paper is conceptually similar to the renormalization-group method (see discussion of cluster renormalization in Secs. III and IV). It is also interesting to note that Wilson[13] refers to the molecular bond in large molecules as a possible area of application of the renormalization-group method. Indeed, the electronic structure of large molecules has been the principal domain of application of the SCF-$X\alpha$-SW molecular-orbital technique.[17,32,33] However, the SCF-$X\alpha$-SW cluster molecular-orbital method is significantly more rapidly convergent in "real space" than the renormalization-group method, as normally implemented in the Kondo problem, because chemical bonding effects between the impurity and successive surrounding shells of atoms are accurately represented in the former approach, whereas in the latter method such effects are not included. As we have shown in Sec. IV, only the nearest- and second-nearest-neighbor shells are necessary to satisfy the cluster sum rule and to yield discrete spin orbitals around the Fermi level that describe the local magnetic moment and the chemical physics underlying the coupling of this moment to the crystal conduction band. Indeed, the existence of a single $CuCu_{12}Cu_6$ cluster molecular orbital, $3a_{1g}(1/2)$ (see Fig. 1), that is, the discrete "real-space" analog of the half-filled conduction band of crystalline copper around the Fermi energy (see discussion of Sec. III) can be viewed simplistically as being equivalent to summing over "many energy scales" of the conduction band in "$\vec{k}$ space," as carried out in the renormalization-group method. However, this statement has not yet been proven rigorously.

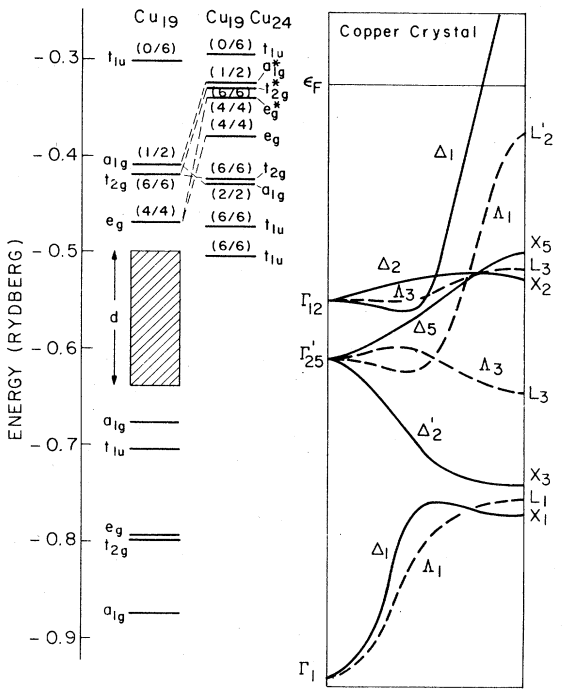

FIG. 18. Comparison of the electronic structure of a $Cu_{19}Cu_{24}$ cluster, as determined by a computational procedure analogous to that of the renormalization-group method, with the electronic structure of Cu_{19} cluster and the band structure of crystalline copper. The results for the 19-atom cluster are the same as those shown in Fig. 1. Note that the character, ordering, and occupancies of the highest three occupied orbitals (e_g^*, t_{2g}^*, a_{1g}^*) for the 43-atom cluster are identical, except for a scale factor, with those of the highest three occupied orbitals for the 19-atom cluster, and the orbital occupancies satisfy the same sum rule, suggesting a "fixed point" in analogy to the renormalization-group method (see text).

As partial support for these claims, we consider the effects of adding the next shell of 24 Cu atoms on the electronic structure of the 19-atom $CuCu_{12}Cu_6$ cluster representing pure crystalline copper, discussed in Sec. III and displayed in Fig. 1. These calculations have been carried out within the framework of the SCF-$X\alpha$-SW molecular-orbital method by a procedure analogous to the renormalization-group technique of considering the Hamiltonian H_{N+1} as a perturbation on the Hamiltonian H_N, including only the most important con-

tributions of the 24-atom shell to the cluster electronic structure around the Fermi level. The resulting electronic structure of the 43-atom $Cu_{19}Cu_{24}$ cluster is compared with the Cu_{19} electronic structure and band structure of crystalline copper in Fig. 18 (cf. Fig. 1). The main effect of the 24-atom shell is to split the highest three occupied orbitals (a_{1g}, t_{2g}, e_g) of Cu_{19} into bonding (a_{1g}, t_{2g}, e_g) and antibonding ($a_{1g}^*, t_{2g}^*, e_g^*$) groups and to introduce two t_{1u} levels, yielding a manifold of discrete levels corresponding to the conduction bands (e.g., Δ_1 and Λ_1) between the top of the d band and Fermi level. The additional orbitals of the $Cu_{19}Cu_{24}$ cluster are just sufficient to accomodate the additional 24 valence 4s electrons of the outer 24-atom Cu shell. The energy-level splittings in going from a Cu_{19} cluster to a $Cu_{19}Cu_{24}$ cluster are analogous to the splittings of the energy scales in going between the successive effective Hamiltonians H_N and H_{N+1} in the renormalization-group method,[13] including the change in scale of the highest three occupied levels. Moreover, the electron configuration of the highest three occupied $Cu_{19}Cu_{24}$ cluster molecular orbitals ($e_g^*, t_{2g}^*, a_{1g}^*$), which transform respectively like $(d_{z^2}, d_{x^2-y^2})^4(d_{xy}, d_{yz}, d_{xz})^6(s)^1$ on the central atom, is identical to that for the Cu_{19} cluster, yielding the "renormalized-atom" $(3d)^{10}(4s)^1$-like configuration and satisfying the cluster sum rule described in Secs. III and IV. This result, including the change in scale factor, can be viewed as being analogous to the occurrence of a "fixed point" or "limit cycle" in a renormalization-group treatment of the Kondo problem,[13] which, however, normally requires many iterations over successive effective Hamiltonians H_{N-1}, H_N, H_{N+1} or over many shells surrounding the impurity in the latter method. Since the three highest occupied cluster orbitals, $e_g(d_{z^2}, d_{x^2-y^2})$, $t_{2g}(d_{xy}, d_{yz}, d_{xz})$, and $a_{1g}(s)$, determine the net magnetic moment and its coupling to the conduction band via the half-filled $a_{1g}(s)$ orbital when a transition-metal impurity (e.g., Ni, Fe, Mn) is substituted for the central Cu atom, these preliminary studies suggest that, except for a scale factor, additional shells of Cu atoms do not alter the essential features of the physical model for local magnetic moments and Kondo effects presented in Sec. IV C. This finding is consistent with our original conjecture, based on simple ideas of coordination chemistry, that for fcc crystalline copper and isolated transition-metal impurities substituted therein, a "coordinatively-saturated" 19-atom cluster is adequate for describing the "renormalizing" effects of the crystalline environment. Nevertheless, we are continuing our studies of the effects of going to successively larger clusters by a computational procedure analogous to the renormalization-group method and the effects of alternative boundary conditions on the clusters.

VIII. EXTENSIONS OF CLUSTER MOLECULAR-ORBITAL STUDIES TO OTHER DILUTE-ALLOY SYSTEMS

A. Impurity-impurity interactions

Many experimental studies of so-called dilute alloys are not carried out in the ideal limit of isolated impurities, but rather at concentrations where there is a high probability that a transition-metal impurity atom will have another impurity atom as its nearest or second-nearest neighbor.[1-3] In view of the above-described key role of chemical bonding-antibonding interactions of an isolated transition-metal impurity with its local environment in an otherwise perfect copper host, it is likely that bonding and antibonding interactions between neighboring impurities would also be key to understanding the measured physical properties of transition-metal impurities in metallic hosts at somewhat higher concentrations, e.g., evidence for the formation of "impurity bands" in photoelectron emission spectra of CuNi alloys (10–15-at. % Ni)[44,45] and the trend of the Kondo resistence minimum toward higher temperatures in CuMn alloys with increasing Mn concentration.[3]

Preliminary SCF-$X\alpha$-SW molecular-orbital calculations for alloy cluster configurations in which the host metal atoms are arranged more or less symmetrically around two interacting transition-metal impurities indicate that such studies of impurity-impurity electronic structure and spin polarization (e.g., exchange enhancement) are practical. It would be especially interesting to observe how the local magnetic moment of an isolated Fe impurity in a copper host, as exemplified by the small exchange splitting in Fig. 12, gradually evolves to the collective "ferromagnetic" moment of an iron cluster, as exemplified by the large exchange splitting of energy levels for Fe_9 and Fe_{15} clusters in Figs. 6 and 7, respectively, of the last paper in Ref. 23, as Fe atoms are substituted for Cu atoms.

B. Transition-metal impurities in aluminum

In Sec. II, we briefly described recent SCF-$X\alpha$-SW studies of aluminum clusters and chemisorption thereon, carried out by Messmer and coworkers.[24,25] Using their findings as a starting point and 13-, 19-, and 43-atom clusters that represent the local molecular environment up to third-nearest neighbors in fcc crystalline aluminum, we have begun SCF-$X\alpha$-SW studies of the electronic structures of transition-metal impurities in aluminum, a dilute alloy system that has

run a close second to the above-described copper-based system with regard to broad experimental and theoretical interest.[1-3] The problem of transition-metal impurities in aluminum is especially well suited for the study of successively larger cluster models in connection with the renormalization-group method discussed in Sec. VII, because the absence of d orbitals on the Al atoms leads to smaller secular determinants and correspondingly less computer time in the SCF-$X\alpha$-SW method than for copper.

Preliminary cluster models for Ni, Fe, and Mn impurities in aluminum are consistent with the absence of permanent local magnetic moments,[1-3] with the single-peaked behavior of the impurity resistivity versus the impurity atomic species[1-3] (as compared with the double peak for these impurities in a copper host shown in Fig. 14), and with recently measured photoelectron spectra.[59] Whereas in a copper host, the transition-metal impurity electronic structure is governed by bonding-antibonding interactions between the impurity d orbitals and sd-hybrid orbitals on the surrounding Cu atoms, in an aluminum host such interactions occur between the transition-metal impurity d orbitals and sp-hybrid orbitals on the surrounding Al atoms, the localized p orbitals of Al playing much the same role as the localized d orbitals of Cu.

To the extent that the cluster molecular orbitals around the Fermi energy, in conjunction with the transition-state concept, can reveal the onset of localized spin fluctuations, as discussed in Sec. IV C for Fe and Mn impurities in a copper host, preliminary SCF-$X\alpha$ cluster models for Mn impurities in an aluminum host, where localized spin fluctuations have been speculated to occur,[1-3] indicate the presence of available empty antibonding Mn-impurity d orbitals near the Fermi energy. These results will be the subject of a future publication.[60]

C. Fe impurities and "giant magnetic moments" in palladium

One of the most interesting yet poorly understood phenomena associated with magnetic impurities is the occurrent of giant magnetic moments for Fe impurities in transition-metal hosts such as palladium.[1] Moments as large as ~12 μ_B per Fe atom in palladium have been observed. The generally accepted notion is that the giant moment arises from exchange enhancement and long-range polarization of the host metal. In view of our finding that the nearest- and second-nearest-neighbor environment is adequate for describing the local magnetic moments and Kondo effect of Fe impurities in copper, it would be interesting to see whether the spin-polarized electronic structure of a $FePd_{12}Pd_6$ cluster simulating the local environment of an Fe impurity in fcc crystalline palladium is sufficient to describe the onset of the giant magnetic moment. Our conjecture is that strong coordination chemical bonding-antibonding interactions of the Fe impurity d spin orbitals with the d spin-orbitals on the surrounding Pd atoms, similar to effects described in Sec. IV, are largely responsible for the giant net spin polarization. SCF-$X\alpha$-SW molecular-orbital studies have already been carried out successfully for Pd clusters containing up to 13 atoms, including relativistic effects (see Sec. II and Refs. 19 and 20), and similar calculations for the 19-atom clusters, $PdPd_{12}Pd_6$ and $FePd_{12}Pd_6$, are in progress.

D. Rare-earth impurities in metallic hosts

Kondo-like anomalies in the physical properties (e.g., magnetic susceptibility, electrical resistivity, specific heat, etc.) of metallic systems containing rare-earth ions are often observed in both the dilute-impurity limit and for higher concentrations of the rare-earth element.[61] Curie-Weiss-like magnetic behavior is typically observed above a characteristic temperature (the "Kondo temperature") and is quenched in a fashion not unlike that shown in Figs. 15(b) and (c). The Kondo-like anomalies in the dilute-impurity limit are usually attributed to an antiferromagnetic exchange interaction of the form given in expression (12), where $\vec{S}$ is the impurity spin (due to $4f$ electrons rather than $3d$ electrons) and $\vec{s}$ is the conduction-electron spin of the host metal at the impurity site. In the limit of higher rare-earth concentration, these anomalies are often ascribed to valence or interconfiguration fluctuations.

Although the $4f$ electrons of the rare-earth ions are considerably more spatially localized that the $3d$ electrons of transition-metal impurities, chemical bonding effects with the local crystalline environment are not likely to be negligible in the former case, suggesting that cluster models of the type described in preceding sections would be appropriate for study. Indeed, recent SCF-$X\alpha$-SW molecular-orbital studies of La, Ce, Nd, and Yb rare-earth coordination complexes[62] and of the uranyl ion (UO_2^{2+}) (Ref. 63) show that while the f electrons are largely localized, chemical bonding-antibonding interactions with the surrounding ligands are not negligible and are key to the understanding of measured physical properties. The calculations for the uranyl ion[63] are fully relativistic and show the importance of spin-orbit splittings of orbital energy levels of the type discussed in Sec. VI and illustrated in Fig. 15(a). Moreover, the SCF-$X\alpha$-SW results for both the rare-earth

complexes[62] and uranyl ion[63] are in good quantitative agreement with measured valence photoelectron spectra, satellite structure in core photoelectron spectra, and valence optical-absorption spectra, suggesting that this theoretical approach is not only feasible for coordination complexes or clusters representing rare-earth impurities and their local crystalline environments but can also yield results comparable with experiment. Specific applications of this approach to rare-earth impurities in metallic hosts are planned.

IX. CONCLUSIONS

In this paper, we have attempted to show that the electronic structures of dilute transition-metal impurities alloyed in a noble-metal (copper) host are dominated by local chemical bonding effects arising from the interaction of the impurity d orbitals with dsp-hybrid orbitals on the nearest and second-nearest neighboring host metal atoms, in analogy to metal-ligand interactions in coordinatively-saturated transition-metal complexes. These results provide a new conceptual basis for interpreting the local magnetic moments, residual electrical resistivities, and other physical properties of such transition-metal impurities, and further suggest that previous theoretical models which view the impurity atomic d orbitals as interacting primarily with the delocalized s-like conduction electrons of the host metal yield an unrealistic physical picture.

Nevertheless, the reader (especially one who is accustomed to thinking of the magnetic impurity problem in terms of the traditional $\vec{k}$-space representation of solid-state physics and many-body theory) may have serious doubts about the efficacy of the real-space cluster representation of this problem. Indeed, a skeptic may well be justified in asking how we know that the claimed consequences of the SCF-$X\alpha$ cluster model are authentically physical and not mere serendipitous results of the combination of a density-functional approximation to exchange and correlation (the $X\alpha$ method) which lacks truly rigorous formal theoretical foundation with an ansatz (the cluster) which is a radical abstraction from the physical system. Other than to point out (i) the current state of our understanding of the fundamental basis of the $X\alpha$ method,[14,15] (ii) the many successful applications (in these institutions and elsewhere) of the SCF-$X\alpha$ cluster method to polyatomic molecules, transition-metal coordination complexes, solids, and surfaces (see Sec. II), and (iii) the correspondence between metal cluster electronic structure and crystal band structure (see Sec. III), we may not be able to respond satisfactorily to such a criticism.

However, we can suggest possible routes to a more formal understanding of this theoretical approach which may eventually satisfy even the most severe critic. In Sec. VII, we have described possible conceptual and computational relationships between the real-space cluster method and the renormalization-group method of attacking the Kondo problem. It is often claimed[13] that the renormalization-group technique is tied up with the formal concepts of "universality" and "scaling," namely, that the physical properties of a system described by a "fixed point" are independent of the parameters in the initial Hamiltonian. It is conceivable that results obtained with the SCF-$X\alpha$ cluster method can also be understood in terms of these concepts. We have demonstrated that a coordinatively saturated 19-atom cluster yields discrete molecular spin orbitals around the Fermi energy which satisfy a sum rule and account for the renormalizing effects of impurity-host coupling that are most directly pertinent to the observed local magnetic moments and residual resistivities. The fact that these levels maintain their relationships in a 43-atom cluster which includes the third-nearest neighboring shell of atoms, except for a rescaling of their energies, indeed suggests that the connections of the cluster electronic structure and associated properties to those of the infinite solid can be understood in terms of scaling and universality. Unfortunately, this is largely speculation at the present time, and further work will have to be carried out to verify these connections.

Finally, the SCF-$X\alpha$ cluster method is a one-electron technique somewhat analogous to Fermi-liquid theory (see Sec. IV C), whereas the Kondo problem and the application of renormalization-group theory (as well as other theoretical approaches) to this problem are usually viewed as many-electron situations. Nevertheless, if the present cluster molecular-orbital description of the Kondo problem ultimately proves to be incomplete, there are reasonably well-defined routes to constructing many-electron states from the one-electron eigenstates obtained by the SCF-$X\alpha$ method, specifically via configuration interaction or many-body perturbation theory. In other words, cluster impurity molecular-orbital configurations like those shown in Fig. 12 and 13, in conjunction with the transition-state procedure,[14,15] can be used as the basis for calculating many-electron multiplet states. Conversely, SCF-$X\alpha$ cluster molecular-orbital configurations can be shown rigorously to be equivalent to averaging over multiplet states.[14] Alternatively, one

can use the cluster eigenstates as a more realistic starting point for many-body perturbation theory than the traditional impurity atomic orbital and free-electron (plane-wave) bases. These suggestions are a matter for future investigation, and we shall not elaborate on them here.

ACKNOWLEDGMENTS

K. H. J. and R. P. M. are very grateful to Frank Ham for carefully reading the manuscript and for valuable suggestions, especially in regard to the discussion of Jahn-Teller and spin-orbit effects. K. H. J. is grateful to Peter Wolff for helpful discussions of the magnetic-impurity problem, in particular for suggesting the possibility of reformulating the Anderson Hamiltonian. K. H. J. and D. D. V. have also benefited from conversations with David Adler, P. W. Anderson, Robert Birgeneau, James Bray, Henry Ehrenreich, Alan Heeger, John Joannopoulos, Bruce Patton, and Clifford Shull. Sponsorship of this research at MIT by the N. S. F. is gratefully acknowledged.

---

*Research at MIT sponsored by the NSF, Grant No. DMR-74-15224.

[1]A. J. Heeger, in *Solid State Physics*, edited by F. Seitz, D. Turnbull, and H. Ehrenreich (Academic, New York, 1969), Vol. 23, p. 283.

[2]Various articles in *Magnetic Properties of Metallic Alloys*, Vol. V of *Magnetism*, edited by G. T. Rado and H. Suhl (Academic, New York, 1973).

[3]G. Grüner, Adv. Phys. 23, 941 (1974).

[4]J. Friedel, Can. J. Phys. 34, 1190 (1956); J. Phys. Radium 19, 573 (1958); Suppl. Nuovo Cimento VII, 287 (1958).

[5]P. W. Anderson, Phys. Rev. 124, 41 (1961).

[6]P. A. Wolff, Phys. Rev. 124, 1030 (1961).

[7]J. R. Schrieffer, J. Appl. Phys. 38, 1143 (1967).

[8]L. L. Hirst, Phys. Kondens, Materie 11, 255 (1970); Z. Phys. 241, 9 (1971).

[9]J. Kondo, same as Ref. 1, p. 183.

[10]J. Kondo, Progr. Theor. Phys. (Kyoto) 32, 37 (1964).

[11]C. Stassis and C. G. Shull, Phys. Rev. B 5, 1040 (1972); M. H. Dickens, C. G. Shull, W. C. Koehler, and R. M. Moon, Phys. Rev. Lett. 35, 595 (1975).

[12]J. B. Boyce and C. P. Slichter, Phys. Rev. Lett. 32, 61 (1974); Phys. Rev. B 13, 379 (1976); J. C. Cohen and C. P. Slichter, Phys. Rev. Lett. 40, 129 (1978).

[13]K. G. Wilson, Rev. Mod. Phys. 47, 443 (1975); Adv. Math. 16, 170 (1975).

[14]J. C. Slater and K. H. Johnson, Phys. Rev. B 5, 844 (1972); K. H. Johnson and F. C. Smith, Jr., *ibid.* 5, 831 (1972); J. C. Slater and K. H. Johnson, Physics Today 17, 34 (1974).

[15]J. C. Slater, in *Advances in Quantum Chemistry*, Vol. 6, edited by P. -O. Löwdin (Academic, New York, 1972) p. 1; J. C. Slater, *The Self Consistent Field for Molecules and Solids*, Vol. 4 of *Quantum Theory of Molecules and Solids* (McGraw-Hill, New York, 1974).

[16]K. H. Johnson, J. Chem. Phys. 45, 3085 (1966); K. H. Johnson, in *Advances in Quantum Chemistry*, edited by P. -O. Löwdin (Academic, New York, 1973), Vol. 7, p. 143.

[17]K. H. Johnson, in *Annual Review of Physical Chemistry*, Vol. 26, edited by H. Eyring, C. J. Christensen, and H. S. Johnston (Annual Reviews, Palo Alto, California, 1975), p. 39.

[18]R. P. Messmer, C. W. Tucker, Jr., and K. H. Johnson, Chem. Phys. Lett. 36, 423 (1975).

[19]R. P. Messmer, S. K. Knudson, K. H. Johnson, J. B. Diamond, and C. Y. Yang, Phys. Rev. B 13, 1396 (1976).

[20]R. P. Messmer, D. R. Salahub, K. H. Johnson, and C. Y. Yang, Chem. Phys. Lett. 51, 84 (1977).

[21]M. Moskovits and J. E. Hulse, J. Chem. Phys. 67, 4271 (1977).

[22]G. A. Ozin, Catal. Rev. (to be published).

[23]C. Y. Yang, Ph.D thesis (Massachusetts Institute of Technology, June 1977) (unpublished); C. Y. Yang and K. H. Johnson (unpublished); preliminary results for Fe_9 and Fe_{15} clusters presented in the following review articles: K. H. Johnson, Int. J. Quantum Chem. 11S, 39 (1977); Crit. Rev. Solid State Sci. 7, 101 (1978).

[24]R. P. Messmer and D. R. Salahub, Chem. Phys. Lett. 49, 59 (1977); D. R. Salahub and R. P. Messmer, Phys. Rev. B 16, 2526 (1977); R. P. Messmer and D. R. Salahub, *ibid.* 16, 3415 (1977).

[25]R. P. Messmer, D. R. Salahub, and J. W. Davenport, Chem. Phys. Lett. 57, 29 (1978).

[26]J. W. Davenport, Phys. Rev. Lett. 36, 945 (1976); Ph.D. thesis (University of Pennsylvania, 1976) (unpublished).

[27]D. Dill and J. L. Dehmer, J. Chem. Phys. 61, 692 (1974).

[28]F. A. Cotton and G. Wilkinson, *Advanced Inorganic Chemistry*, 3rd ed. (Interscience, New York, 1972).

[29]L. E. Orgel, *An Introduction to Transition-Metal Chemistry* (Methuen, London, 1966).

[30]K. H. Johnson and F. C. Smith, Jr., Phys. Rev. B 5, 831 (1972).

[31]C. Y. Yang, K. H. Johnson, R. H. Holm, and J. G. Norman, Jr., J. Am. Chem. Soc. 97, 6596 (1975).

[32]D. A. Case, Ph.D. thesis (Harvard University, June 1977) (unpublished); D. A. Case, B. H. Huynh, and M. Karplus, J. Am. Chem. Soc. 99, 6103 (1977).

[33]D. A. Case and M. Karplus, J. Am. Chem. Soc. 99, 6182 (1977).

[34]R. P. Messmer and G. D. Watkins, Phys. Rev. Lett. 25, 656 (1970); Phys. Rev. B 7, 2568 (1973); G. D. Watkins and R. P. Messmer, Phys. Rev. Lett. 32, 1244 (1974).

[35]L. A. Hemstreet, Phys. Rev. B 15, 834 (1977).

[36]D. E. Ellis, G. A. Benesh, and E. Byrom, Phys. Rev. B 16, 3308 (1977).

[37]For a review of theories of alloy electronic structure, see H. Ehrenreich and L. M. Schwartz, in *Solid State Physics*, edited by H. Ehrenreich, F. Seitz, and D. Turnbull (Academic, New York, 1976), Vol. 31, p. 149.

[38]D. House, B. L. Gyorffy, and G. M. Stocks, J. Phys. 35, C4-75 (1974).

[39]P. Lloyd, Proc. R. Soc. (Lond.) 90, 207 (1967); 90, 217 (1967).

[40]J. C. Slater, *The Self Consistent Field for Molecules*

and Solids, Vol. 4 of *Quantum Theory of Molecules and Solids* (McGraw-Hill, New York, 1974), p. 117.
[41]B. Segall, Phys. Rev. 125, 109 (1962).
[42]G. A. Burdick, Phys. Rev. 129, 138 (1963).
[43]L. Hodges, R. E. Watson, and H. Ehrenreich, Phys. Rev. B 5, 3953 (1972).
[44]D. H. Seib and W. E. Spicer, Phys. Rev. B 2, 1694 (1970).
[45]B. L. Gyorffy, G. M. Stocks, W. M. Temmerman, R. Jordan, D. R. Lloyd, C. M. Quinn, and N. V. Richardson, Solid State Commun. 23, 637 (1977).
[46]A. Bansil, L. Schwartz, and H. Ehrenreich, Phys. Rev. B 12, 2893 (1975).
[47]F. S. Ham, J. Phys. Suppl. 32, C1-952 (1971).
[48]P. W. Anderson, *Concepts in Solids* (Benjamin, New York, 1964), p. 126.
[49]R. P. Messmer and D. R. Salahub, J. Chem. Phys. 65, 779 (1976).
[50]H. P. Myers, L. Walldén, and A. Karlsson, Philos. Mag. 18, 725 (1968).
[51]C. Norris and L. Walldén, Solid State Commun. 7, 99 (1969).
[52]J. W. Davenport, W. Ho, and J. R. Schrieffer, Phys. Rev. B 17, 3115 (1978).
[53]M. Kotani, J. Phys. Soc. Jpn. 4, 293 (1949).
[54]J. H. Van Vleck, *Electric and Magnetic Susceptibilities* (Oxford U. P., Oxford, 1932).
[55]F. Herman and S. Skillman, *Atomic Structure Calculations* (Prentice-Hall, New Jersey, 1963).
[56]J. E. Van Dam, P. C. M. Gubbens, and G. J. Van den Berg, Physica 61, 389 (1972).
[57]K. D. Schotte and U. Schotte, Phys. Rev. B 4, 2228 (1971).
[58]B. N. Figgis, Nature 182, 1568 (1958).
[59]P. Steiner, H. Höchst, and S. Hüfner, J. Phys. F 7, L105 (1977).
[60]D. Vvedensky, K. H. Johnson, and R. P. Messmer (unpublished).
[61]See various articles in *Valence Instabilities and Related Narrow Band Phenomena*, edited by R. D. Parks (Plenum, New York, 1977).
[62]J. Weber, H. Berthou, and C. K. Jørgensen, Chem. Phys. Lett. 45, 1 (1977); Chem. Phys. 26, 69 (1977).
[63]C. Y. Yang, K. H. Johnson, and J. A. Horsley, J. Chem. Phys. 68, 1001 (1978).